



5 **Summertime Arctic Aircraft Measurements during ACCACIA**

Hazel M. Jones¹, Gillian Young², Thomas W. Choularton¹, Keith N. Bower¹, Thomas Lachlan-Cope², Sebastian O'Shea¹, James Dorsey³, Russell Ladkin², Amélié Kirchgaessner², Alexandra Weiss²

¹CAS, SEES, University of Manchester, UK

²British Antarctic Survey, High Cross, Madingley Road, Cambridge CB3 0ET, UK

10 ³National Centre for Atmospheric Science, University of Manchester, Manchester, UK

Correspondence to: Hazel M. Jones (Hazel.Jones@manchester.ac.uk)

Abstract. Arctic Climate is not represented with a high degree of certainty in current climate; part of this is due to Arctic clouds not being well modelled. There have been very few in-situ measurements in the region until recent years, where coverage still remains sparse. Whilst a lot is known regarding lower latitude cloud microphysics, the same cannot be said for Arctic cloud microphysics where cloud interactions and feedback mechanisms are known to vary from those at lower latitudes. This paper reports data from the 2013 ACCACIA project where aerosol and cloud data were collected over eight flights sampling in the region around Svalbard during July.

Clouds from six out of the eight flights were found to be mixed phase to some extent, with in-cloud flight-mean droplet number concentrations ranging from 21.7 – 132 cm⁻³ across all flights where clouds were sampled between 262 and 283 K. Cloud droplet diameter was found to increase from cloud base to cloud top within sampled stratocumulus layers which were noted to lift and deepen when moving out from over the sea-ice to over the open ocean. Cloud ice particles concentrations, when present, ranged from 0.42 – 0.88 L⁻¹, with irregular, stellar and columnar habits noted. Results suggest a small number of ice nucleating particles were active in the region, with conditions intermittently present such that secondary ice processes were able to glaciare small portions of the cloud.

The purpose of this paper is to provide a more extensive range of data for the development of improved parameterisations for use in models applied to Polar regions.

1 Introduction

The current lack of understanding of Arctic cloud processes and feedback mechanisms limits the ability of climate models to accurately predict the current climate in this region which, which in turn, limits the ability to provide accurate regional weather forecasts. The Arctic climate is rapidly changing, causing increased scientific interest in this region. Current climate models have significant problems with the Arctic (e.g. ACIA, 2005), with the IPCC reporting the largest end-of-century inter-model spread in climate projections for this region. The Polar Regions have environmental characteristics very different



5 to mid-latitudes and so have a unique response to the warming atmosphere (Tjernstrom et al. 2004). To date, there have only
been a limited number of Arctic projects making the focused in-situ aircraft measurements of cloud microphysical data
required to enable the development of parameterisations for use in the climate and forecast models. Figure 1 highlights the
Arctic regions covered by some of these past experiments, along with the region covered by this work. The relatively short
observation periods of aircraft campaigns cannot be used to investigate climatic trends, but they can provide a more detailed
10 study of the important processes that need to be understood to develop the required parameterisations. Conditions in these
shorter timescale measurement periods must be compared against the longer term trends in the area to know how
representative of the Arctic they may be.

As is evident from Fig. 1, there is not complete coverage of in-situ data, with very few measurements in the central Arctic
region. For this central region, current parameterisations are based on remote sensing data from satellites; this in itself is
15 problematic due to the lack of in-situ observations for developing and testing the remote sensing techniques in the Arctic.

From past observations it is known that low-level mixed-phase clouds (MPCs) are ubiquitous in the Arctic, particularly
during the summer months where average cloud fraction can be 80-90% (e.g. Shupe et al. 2011). Mioche et al. (2015), using
satellite remote sensing, showed a large occurrence of MPCs all year, particularly in the Svalbard region, persisting for
several days under a variety of conditions. These clouds have a substantial effect on the surface energy budget (e.g. Sedlar et
20 al. 2011), and so changes in Arctic cloud cover could have a notable impact on the change in perennial Arctic sea ice (Kay
and Gettelman, 2009). These Arctic low-level clouds differ from those at lower latitudes as they tend to warm the surface
relative to clear conditions most of the year (e.g. Tjernstrom et al 2004) due to the balance between the optical properties of
the cloud and the highly reflective sea-ice surface (e.g. Sedlar et al 2011). The MPCs occur as single or multiple stratiform
layers, mainly consisting of supercooled droplets near cloud top where ice crystals form and eventually precipitate, with
25 some noted as continually precipitating (Mioche et al 2017). However, when modelling these clouds, liquid and ice are
typically assumed to be uniformly mixed throughout model grid boxes (e.g. Tan et al., 2016).

Single layer Arctic MPCs are characterised by increasing values of liquid water content (LWC) with altitude along with a
slight increase in droplet diameter from cloud base to cloud top. Mioche et al. 2017 reports spring time mean LWC values in
the Svalbard region between 0.1 (bottom of liquid layer) and 0.2 gm^{-3} (cloud top), with a mean cloud droplet concentration
30 of around 120 cm^{-3} almost constant throughout the layers (with smaller values observed near cloud top). Mean ice crystal
concentration for the same study was reported as 3 l^{-1} with no height correlation, though concentrations reduced to zero at
cloud top, meaning cloud tops consisted of almost 100 % supercooled liquid droplets. The dominant ice habit was reported
to be rimed and irregular within the MPCs and a significant number of plates and stellar crystals were present regardless of
the cloud layer altitude. Similar results have been reported in the western arctic (e.g. ISDAC - McFarquhar et al. 2011), with
35 the added presence of a notable fraction of needles and columns (McFarquhar et al. 2007). Higher mean values were seen for



5 SORPIC, the more recent of the studies used in Mioche et al. 2017, with a mean droplet concentration of 300 cm^{-3} and 0.3 gm^{-3} LWC. SORPIC average ice crystal number concentrations were around 3 l^{-1} , with IWC values from 0.01 to 0.035 gm^{-3}

Previous studies have found evidence for secondary ice production within Arctic MPCs; namely the Hallett-Mossop (H-M) process (Hallet and Mossop, 1974) as presented in Lloyd et al. 2015, and the shattering of large drops during freezing (e.g. Gayet et al. 2009).

10 Another notable characteristic of Arctic MPCs is that they can persist for several days (e.g. Morrison et al. 2012) and do so under a variety of meteorological conditions making them distinct from mid-latitude MPCs which glaciate readily through the Wegener-Bergeron-Findeisen (WBF) process; this is due to the paucity of IN in the Arctic.

Detailed observations of the Arctic atmosphere using direct measurement techniques, providing high spatial resolution data ($<100 \text{ m}$), are required to increase our understanding of the many processes unique to this remote environment that are difficult to investigate in-situ. The Aerosol-Cloud Coupling And Climate Interactions in the Arctic (ACCACIA) campaign was designed to address these issues and was split into two parts: Spring (Mar-Apr 2013) and Summer (July 2013). Flights were conducted in the European Arctic close to Svalbard. The overall objective of the campaign was to increase our current understanding of Arctic cloud-aerosol interactions and their effects on the regional climate. This paper aims to give an overview of the cloud microphysics and aerosol data collected during the eight science flights of the summer campaign.

20 **2. Instrumentation:**

2.1 The MASIN aircraft

The British Antarctic Survey (BAS) operate the Meteorological Airborne Science INstrumentation (MASIN) flown on the BAS Twin Otter VP-FAZ. ACCACIA was the first Arctic program for the aircraft. The aircraft flies at $\sim 60 \text{ ms}^{-1}$ for data collection, over an altitude range from near surface up to $\sim 5000 \text{ m}$ (limited by having an unpressurised cabin). The lower flying limit can range from 30 to 150 m depending on the flight path, surface type and visibility.

2.2 Meteorological instrumentation

3-D winds were recorded at 50Hz using a nine-hole Best Aircraft Turbulence (BAT) probe (Garman et al., 2006) boom-mounted above the cockpit and which extends forward of the aircraft nose. This probe incorporates dynamic and pressure sensors. Static and dynamic pressure were measured (at 5Hz) via the aircraft static ports and heated Pitot tube using Honeywell HPA sensors.

Position, altitude and velocity were recorded using an OXTS Inertial+ GPS linked inertial navigation unit. An explanation of calculations and corrections applied is given in King et al., 2008. Fiedler et al. 2010 also provides details of the MASIN core instrumentation.



5 Non-deiced temperature was measured by a Goodrich Rosemount 102E4AL, and deiced temperature with the 102AU1AG model. Both probes were mounted on the nose of the aircraft and logged at 0.7 Hz.

A Buck 1011C cooled mirror hygrometer was fitted on the aircraft nose with the mirror temperature recorded at 1 Hz with ± 0.5 K uncertainty depending on the variability in conditions. This instrument measures the atmospheric dew-point using the chilled mirror technique: air is passed over a mirror-like metal surface and the temperature regulated until condensation
10 begins to form on the surface, this being the dew or frost point.

2.3 Cloud microphysical instrumentation

A DMT Cloud Droplet Probe (CDP-100) was mounted under the aircraft nose, measuring droplets in the range $3 < d_p < 50$ μm . Particle size is calculated from the intensity of the forward-scattered laser light ($4\text{--}12^\circ$) using Mie scattering solutions (Lance et al., 2010). Liquid Water Content (LWC) and mean effective radius (RE) can be derived from the CDP measurements
15 assuming liquid spheres.

A wing-mounted Droplet Measurement Technologies (DMT) Cloud, Aerosol, and Precipitation Spectrometer (CAPS) probe (Baumgardner et al., 2001) was also deployed in ACCACIA. It combines multiple instruments into one flight canister. It comprises a Cloud Imaging Probe (CIP-25), a Cloud and Aerosol Spectrometer (CAS-DPOL) and a hot wire liquid water content (LWC) probe. The CIP is an optical array shadow probe and detects particle in the size range $25 < d_p < 1550$ μm
20 (using a 64 element array with a 25 μm image resolution). The CIP was calibrated using a spinning disk fitted between the probe arms before and after the campaign. The CAS-DPOL is a light scattering probe that detects forward, back-scattered and back-scattered polarised light from particles in the size range $0.5 < d_p < 50$ μm (Glen and Brooks, 2013). Its calibration was checked regularly throughout the campaign using reference glass beads. The Hotwire liquid water content (LWC) probe detects cloud water in the range $0.01 - 3$ gm^{-3} ; it was not calibrated but its output was checked against the total liquid water
25 content calculated by summing the particles observed by the other spectrometer probes.

The Two-Dimensional Stereoscopic Probe (2D-S, Stratton Park Engineering Company Inc. Boulder, USA – Lawson et al., 2006) is a high resolution optical array shadow probe which consists of a 128-element photodiode array with an image resolution of 10 μm . This probe was also wing-mounted (opposite wing). In this study, measurements from the 2D-S probe have been shown in preference to those from the CIP-25 due to the significantly faster response time and higher resolution of
30 the former. (CIP-25 and 2D-S measurements generally compare well, with a greater difference in reported number concentration for flights where ice was present and, in these instances, 2D-S numbers were much higher than the CIP-25). Processing and analysis of this dataset has been discussed previously (Taylor et al., 2016) and here we use the same methodology. Imaged particles are segregated into categories based on their circularity (Crosier et al., 2011). Highly irregular (HI) particles are classified as ice particles, whereas low irregular (LI) particles are classified as droplets. Close
35 attention is paid to the images within the classification to assess the accuracy of classification, and adjustments have been



5 made where necessary. The ‘small’ particle classification is for those particles whose images are not large enough to determine particle type, in this case $< \sim 80 \mu\text{m}$ (for CIP-25 this was $< \sim 140 \mu\text{m}$). Ice water content values are derived from the particle size measurements using the Brown and Francis (1995) mass dimensional relationship; LWC was calculated for the LI category assuming liquid spheres.

10 The 2D-S, CIP-25 and CAS were fitted with anti-shatter tips to reduce ice shattering on the probe arms/inlets (Korolev et al 2011, 2013). Additionally, the inter-arrival time data from the CIP-25 and 2-DS probes has been used to check for any shattering instances (i.e. when very short inter-arrival times (IATs) are recorded). Crosier et al. 2014 outlines the steps of careful analysis of IAT histograms for different cloud microphysical conditions to determine an appropriate threshold to apply to the dataset. For this dataset 2D-S minimum IAT acceptance time was between 1 – 3 μs , and the CIP-25 required no correction.

15 2.4 Aerosol instrumentation

The aerosol inlet on the Twin Otter is a Brechtel Model 1200 (www.brechtel.com); an isokinetic inlet with $>95\%$ transmission efficiency for particles $0.01 - 6 \mu\text{m}$. From this inlet, a TSI 3772 Condensation Particle Counter (CPC) counted airborne particles down to 10 nm at a flow rate of 1 LPM over a concentration range $0 - 10^4 \text{cm}^{-3}$ and a GRIMM 1.109 portable aerosol spectrometer (www.grimm-aerosol.com) also measured larger aerosol particles, in the size range $0.25 - 32 \mu\text{m}$.

In addition to cloud particles, the wing mounted CAS measures aerosol particles in the size range $0.5 < d_p < 50 \mu\text{m}$ using the light intensity from forward and backscattered light from single particles again using Mie Theory (Baumgardner et al., 2001). Data from the CAS in ‘cloud-free’ regions – defined here as when CDP LWC $< 0.01 \text{gm}^{-3}$ – were used to investigate the environmental aerosol properties.

25 2.5 Additional data

The UK Met Office provided high resolution forecasts for the project and these were used, along with Norwegian Met Service charts, for flight planning.

Sea ice cover and fraction was obtained from NASA’s National Snow and Ice Data Centre (NSIDC), derived from passive microwave brightness temperatures (Peng et al., 2013).

30 European Centre for Medium-Range Weather Forecasts (ECMWF) Reanalysis (ERA)-Interim data (Dee et al., 2011) are used on a 0.25 degree latitude/longitude grid at 1200 UTC on the given dates to provide meteorological information about the region. These are shown in the Fig. 3. In addition, derived cloud top height from MODIS satellite retrievals and AVHRR



5 visible satellite images are provided in the supplementary material (supplementary 1, 2) to show the cloud structure in the ACCACIA region.

Back trajectories were obtained using the National Oceanic and Atmospheric Administration (NOAA) Hybrid Single-Particle Lagrangian Integrated Trajectory (HYSPLIT 4.0) model (Draxler and Hess, 1998). Five-day back trajectory paths are shown in this paper, however, it must be noted that there is a degree of uncertainty with the products, turbulent air motions along the derived path are not accounted for (Fleming et al., 2012) and that the data are not plotted further than when the back trajectory intersect the ground.

3. Results

3.1 Meteorology and flight objectives

15 Nine flights were performed during July 2013 as part of the ACCACIA project (see Fig. 2); these comprised of one test flight and eight science flights with varying scientific objectives (see Table 2). Sea ice extent had retreated rapidly during the first half of July 2013, then was much slower for the second half of the month. This was due to a change in weather patterns from being dominated by high pressure and anticyclonic winds at the start to cool conditions and counter clockwise winds. NSIDC data show that Arctic sea ice cover was reduced compared to previous years but that the sea ice edge in this region was only slightly further to the north than the 1981 – 2010 median July, see supplement 2.

20 At the beginning of the campaign, a large area of low pressure was centred on 85° N, 90° E, with several high and low pressure regions found to the south around 75° N (see Fig. 3). Over the course of the project, the low pressure region moved in an anti-clockwise direction around the pole, thus influencing the meteorology in the vicinity of Svalbard. The main high pressure areas were primarily centred over mid-Greenland, over the Northern Canadian islands and over the north of mainland Russia, with this latter area occasionally extending toward the south-west of Norway.

25 The first science flight (identifier M191) was flown on 18 July 2013, during which the aircraft flew on northerly and southerly headings through multi-layered stratocumulus at 15° E between 78.3 and 81.3 °N (Fig. 2 shows the flight tracks of all flights) taking measurements of clouds over both the sea and the sea-ice. The ice-edge in this area was at approximately 81 °N. Westerly winds of up to 20 ms⁻¹ were measured at approximately 3000 m. Cloud top height remained below 2500 m in the investigated region, with higher cloud (>5000 m cloud top) present to the west. A 3 °C temperature inversion was
30 noted around 150 m, with a second inversion around 1200 m of approximately 2 °C associated with the bottom of a dry layer extending up to ~2400 m.

The second science flight (M192) was flown on 19th July 2013 with initial aims to follow a similar flight track to the previous day. By this date, the primary low pressure area had moved to the east (85° N, 150° E) and a secondary low pressure system moved towards Svalbard from over North Scandinavia. High pressure areas dominated between these



5 systems, centred to the North East of Svalbard. Cloud forecasts to the north of Svalbard from the UK Met Office were found to be inaccurate this day as no cloud was found in the intended science area when the aircraft arrived there; therefore, the aircraft diverted to the South East of Svalbard to sample the edge of frontal clouds. Cloud top height data from MODIS (see supplementary data 2) shows cloud top heights of up to 10000 m in this frontal region. Straight and level aerosol runs were performed to the North of Svalbard, distant from the cloud passes. Eastward and northward wind components were mostly
10 $<10 \text{ ms}^{-1}$.

The next science flight (M193, 22nd July) saw the secondary southern low pressure system enter the polar region along the east coast of Greenland. This system was less intense than the primary low pressure area circumnavigating the pole; however, it was positioned much closer to Svalbard and the scientific region of interest. Measurements were made to the north of Svalbard with the aircraft sampling multi-layer stratocumulus. The aircraft flew north from Svalbard to over the sea
15 ice, and subsequently conducted a single run to the west and then the east, before returning to sample over the sea at 80.5° N . This allowed the aircraft to sample part of a cloud system centred on the newly introduced low pressure system in the vicinity of Svalbard. A small temperature inversion around 50 m was briefly sampled, with a higher altitude more notable inversion associated with a dry layer (up to 4° C and 50 % drop in RH over 500 m) around 1700 m sampled several times during the flight. South-westerly winds were noted close to the centre of the low pressure, with the exception of the runs
20 over the sea ice where the winds were south-easterly. Cloud tops were $<2000 \text{ m}$ in the immediate area, though higher cloud was noted to the west and the north-north-east of the flight track.

By 23rd July (flight M194), the smaller low pressure area in the vicinity of Svalbard moved north-eastward across the Northern Russian islands, merging with the primary low pressure region (see Fig. 3d). This system had grown considerably in size and strength and was centred on $85^\circ \text{ N } 150^\circ \text{ W}$. By moving eastwards, these systems allowed high pressure areas to
25 develop in the science region, with particularly high pressure noted over the north of Norway. Flight M194 followed a flight track similar to M191 to sample clouds in the trailing low pressure system; however, in contrast to M191, only a single layer of cloud was sampled. In the main sampling area, across the sea ice edge, cloud tops of up to 6000 m were noted at the northern end, but only up to 2000 m at the southern end. During the runs on northerly and southerly heading near the ice edge, the measured vertical winds were mostly strong downdrafts up to 5 ms^{-1} when around 1000 m and slight updrafts of
30 approximately 2 ms^{-1} when above 2000 m. A temperature inversion of almost 4° C was associated with a dry layer between approximately 1000 and 1500 m. Winds were typically from the west, with the exception of the southerly end of the flight track where south-westerly winds influenced the science region.

By 25th July (flight M195), the two main low pressure systems had combined and continued moving eastward (now centred on $80^\circ \text{ N}, 130^\circ \text{ W}$). A much smaller low developed to the east of Svalbard, south of Franz-Josef-Land, which was
35 surrounded by high pressure regions with centres over Greenland, to the south west of Svalbard, and to the east of Novaya Zemlya (see Fig. 3e). M195 sampled a single cloud layer to the northwest of Svalbard close to the sea ice. A 1° C



5 temperature inversion was noted around 150 m, with a second 1 °C inversion 100 m deep at around 600 m. The wind was south westerly, below 2000m, but became a dominant north westerly above. Satellite images show the sea-ice in the science region was very broken up, and MODIS cloud top height data indicate that no clouds were present at higher altitudes over the region investigated (supplementary material 1).

10 The centre of the main low pressure region moved southwards and eastwards with time through the campaign, reaching 80 °N, 120 °W by 26 July during the 6th flight (M196). The area of low pressure seen to the east of Svalbard on the previous day was still present, now centred on approximately 80 °N, 80 °E. High pressure centres were seen over the Laptev Sea, to the north of Norway and to the south of Greenland. Flight M196 (26 July 2013) saw the aircraft perform flight legs orientated in north-south direction along 15°E, across the sea-ice edge to the North of Svalbard. South-westerly winds were measured throughout the flight. Two temperature inversions were sampled, one at 200 m (1 °C), and a second at 750m (3
15 °C), both associated with a 10 % drop in RH.

By the next flight (M197), the primary low pressure region had moved almost directly north, reaching approximately 85 N, 110W on 29th July and had reduced in size. In addition, a large high pressure region developed over the north of Scandinavia and Russia. The aircraft flew further west than previously in order to fly over the RRS James Clark Ross (JCR) which was collecting sea surface measurements as part of the same project (e.g. Allan et al., 2015). Flying in an approximately
20 triangular path, the aircraft flew west into the science region, then performed a single track run southwards over a section of sea-ice extending down to 76N between Greenland and Svalbard, see Supplementary 3, sampling a single layer cloud in the vicinity of the JCR. A low altitude temperature inversion of 1 °C was noted at the start of the flight at 150 m. A second inversion was noted at 500 m at the northern end of the track, lifting to 1200 m at the southern-most edge of the sea ice “peninsula”. Strong south-easterly winds (~10 ms⁻¹) were measured to the north of the “peninsula”, with much weaker (~2
25 ms⁻¹) southerly winds measured towards the southern end. Satellite imagery shows maximum cloud top in the science area at approximately 1500 m.

By the last flying date (30th July, flight M198), the large low pressure system had weakened considerably while extending across a wider area between 90° W and 180° W. A additional low pressure region began to approach the science region around Svalbard from the south. The widespread high pressure region to the east noted during M197 was still in place over
30 northern Norway. Flight M198 again flew to the west of Svalbard to sample a single cloud layer above the sea ice. North-westerly winds dominated during this flight. A 2 °C temperature inversion from 200 - 400 m was detected in the science region, whilst a second inversion at 1400 m was observed on the transit from the east.

Temperature measurements from all eight flights show a range of 262 – 281 K. Flights M196, M197 and M198 only sampled up to 2500 m, so few data points show temperature readings below 0 °C, with no readings <-3 °C. All other flights have



5 periods when the temperature readings were within the Hallett-Mossop range (-3 °C to -8 °C) within cloud. Only M191, M193, M194 and M195 collected data at temperatures < -8 °C; however, in the case of M193, only for a few minutes.

3.2 Aerosol Measurements

Each flight pattern contained at least one straight and level run (SLR) at low altitude (60 – 400 m, below cloud) and one SLR at higher altitude (1050 – 3380m, typically above clouds) through cloud free air (defined as when CDP total concentration was < 1 cm⁻³). For these time periods, the mean number concentration (and standard deviation) from the GRIMM, CPC and CAS instruments have been reported in Table 3. Back trajectory analyses for these times also reveal information regarding the most likely track of the air on its approach to the science area.

Figure 4 shows time series (from flight M192) of number concentrations from the Grimm and CAS along with the CDP number concentration to indicate cloud location and the calculated RH from the dew point mirror. Average size distributions from the time indicated on the RH time series are shown on the right of the figure.

When the CAS and Grimm are compared, it is important to note that the Grimm was sampling through a heated inlet (with reduced transmission efficiency for particle > 6µm) inside the aircraft, whereas the CAS was sampling externally. The CAS reports more, larger aerosol particles due to measuring the aerosol particles in ambient conditions where they are likely to be swollen under high RH conditions. When the RH of the sampled air is very high (over 85% RH), then there can be big differences between the reported number concentrations from the two probes.

For several flights (M191, M192, M193, M195, M197, and M198) the reported mean GRIMM concentrations were significantly larger for the higher altitude run. M194 and M196 show only a slight increase at the higher level. The highest reading was for the high altitude SLR of M197 where the value of 21.9 cm⁻³ was more than twice the next highest value.

M192, M197 and M198 all show high CPC concentrations for the lower level runs. These were all performed over the sea ice or over the sea ice edge. M197 and M198 (the largest recorded value) were taken in the region where the JCR was operating. The largest GRIMM values detected during M197 were observed at the northern end of the flight track, with the overpass of the JCR occurring at the south-westernmost point of the flight track when low numbers were recorded. During this flight, the wind, as measured on the JCR, was coming from the North-East ~5 ms⁻¹.

3.3 Cloud measurements

As part of this project, several clouds were investigated. Most of the flights (M191, M193, M194, M195, and M196) sampled stratocumulus layers to the north of Svalbard, typically along the longitude of 15° E. M197 and M198 sampled cloud to the west of Svalbard to try to overpass the JCR research ship that was taking measurements as a separate part of ACCACIA. M192 took measurements at the edge of a frontal cloud to the South-East of Svalbard.



5 3.3.1 Stratocumulus Clouds sampled to the North of Svalbard

As detailed in Table 3, flights M191, M193, M194, M195 and M196 were all performed to the north of Svalbard with the majority of the flight tracks following the 15 °E meridian; however, there are differences, with some flights including periods measuring cloud over the sea-ice, see Fig. 2.

10 M191 and M193 saw the aircraft sample multi-layer stratocumulus. M191 was a cloud-focussed flight and has been discussed in detail as a case study in Lloyd et al. (2015). M193 was primarily a surface flux flight. Similar temperature ranges were found for these two flights, see table 2, where cloud was sampled in the Hallett-Mossop temperature range. 2D-S images from these flights show columnar ice crystals were present.

15 Images from M191 show several swift transitions from almost entirely droplets to almost all ice, predominantly of columnar habit. In this case, columns were typically well formed and long enough to touch the edge of the 2D-S array (and thereby categorised as ‘Edge’ particles not ‘HI’ particles). Also present were some irregularly shaped ice crystals; all ice particles showed evidence of riming when detected lower in the cloud. Images from M193 show that the clouds sampled on this day switched from being all liquid to mixed phase with primarily columnar habit crystals, but only one occasion when the cloud was fully glaciated - around 13:10 for ~20 s. The phase frequency plot in Fig. 7 shows the difference in phase distribution between M191 and M193.

20 Large stellar crystals were also observed during M193 in certain areas. As these particles are very large (sometimes exceeding 2500 µm), and mostly touch the edge of the 2D-S array, their numbers are not included in size distribution data – highlighting the need for close inspection of the image data to ensure such information is not lost. These stellar crystals were quite dendritic with planar growth evident on many of them, see Fig. 8.

25 These crystals were seen on three separate occasions, initially at 12:22 for approximately 3 minutes during a profile from 3200 m to 3600 m, see Fig. 8, then just 7 minutes later at 12:33 for around a minute at the start of a descending profile (4300 – 4100 m), then finally 12 minutes later around 1800m for less than a minute during the same descending profile. From Fig. 9 we can see that the stellar crystal regions were co-located at different heights, with the degree of riming and aggregation increasing with descent through the cloud, see Fig. 8.

30 A small number of stellar crystals were also noted in M191 on one occasion. They were observed at the top of a cloud layer around 80° N, 15° W @ ~3400 m around 10:40 when the temperature was ~265 K. This same region was sampled earlier in the flight around 09:10 at 2700 m, though stellar crystals cannot be clearly seen during this cloud pass.

M194, M195 and M196 sampled single cloud layers. For the M195 case, there were several instrument issues throughout the flight such that we can only report the data from times when relevant instruments were known to be working correctly. Cloud was also mostly only seen during transit.



5 M194 was a cloud focussed flight and included two sets of saw tooth profiles investigating a single layer cloud from open water to over sea ice, and vice versa. These data are shown in Fig. 10. The cloud layer deepens as the aircraft approaches the open water. As Fig. 10 shows, ice was detected during this flight. Similar to M191, there were at least two instances of a rapid change in cloud particles from almost all liquid to almost all columnar ice in addition to periods of mixed phase cloud.

10 M196 was also a cloud focussed flight and performed one set of saw-tooth profiles from south to north; however, the aircraft only approached the sea-ice and did not fly directly over it, though it did fly over the marginal ice zone (MIZ) which was quite wide on this day, see supplementary 3. Again we can see the change in cloud top height and depth as the aircraft approached the ice-edge, see Fig. 11. The 2D-S data show that this cloud is virtually all liquid, consistent with the observed temperatures being near 0 °C for this flight. For the cloud layer in M196, the observed cloud base and cloud top was lower in altitude than M194. Cloud droplet size does not vary much as the aircraft sampled closer to the ice edge but CDP LWC
15 values and CDP R_e were higher for this case than for M194.

3.3.2 Clouds sampled to the West of Svalbard

M197 and M198 were conducted to the west of Svalbard. M197 was further south, with the main focus to meet up with the JCR; M198 focussed more on measurements over the sea ice. 2D-S images show that these clouds were almost all liquid phase. CDP number concentrations from the two flights were very similar, as were the meteorological conditions and back.
20 Although the sampling of a cloud layer during M197 was not as extensive as for M194 and M196, a similar lifting of the cloud layer was noted when moving from over sea-ice to over open ocean. The largest CDP R_e values were reported for these flights, likely due to the droplet number being lower. The lack of ice and therefore no WBF process acting to reduce the cloud droplet size could also play a role.

One feature that was evident during M197 was the potential for drastic change in the local temperature inversion over a relatively short distance, see Fig. 12. These profiles were moving from over the ice ‘peninsula’ (P8) to over the open ocean (P10 onwards).
25

3.3.3 Frontal Cloud sampled to the South-East of Svalbard

M192 was a cloud-focussed flight initially intended to be flown to the north of Svalbard, but diverted to the south east as no forecast clouds were found in the intended sampling area. The cloud sampled was at the edge of a strongly layered frontal cloud, which was part of a larger system centred over Scandinavia (see supplementary 2), with cirrus present above. This
30 flight has been discussed as a case study in Lloyd et al. 2015 and, like M191, also noted occasional rapid transitions from liquid cloud to almost fully glaciated clouds. Measurements were found to be consistent with the Hallett-Mossop process occurring.



5 4. Discussion

Arctic stratocumulus layers were sampled at various locations and altitude during the course of the summer campaign of the ACCACIA project. The results from the cloud and aerosol instrumentation reveal a range of conditions present for these clouds. When comparing these results to other campaigns, it must be noted that the Svalbard region, presents a larger occurrence of low-level MPCs compared to the average Arctic (e.g. Mioche et al. 2015) and that the sea-ice cover in this region during July 2013 was the lowest on record, with coverage much lower than the years either side. As in previous projects (e.g. Uttal et al. 2002), on several occasions fog was present at low altitude between the cloud base and the surface sea-ice, which restricted flying at low-level. We are not able to present any cloud microphysics of this fog, which has been shown to have little satellite signature (e.g. Rossow and Garder 1993), as we did not sample it directly due to flight limitations.

15 4.1 Cloud microphysics

As reported in many previous Arctic cloud studies, the clouds present were stratocumulus, either appearing as single layer or multi-layered. Multi-layered clouds are more commonly seen in the summer months, though their exact formation mechanisms are not known (Curry et al. 1996). Arctic clouds are typically reported to have a well-defined inversion at the cloud top, particularly in the winter/spring months, then less well-defined during the summer months when a warmer surface, with stronger short-wave heating from above, can result in a less distinct inversion.

Single layer clouds sampled here presented features noted in the past: predominantly comprised of supercooled water droplets. Droplet concentration, LWC and effective radius all increase from cloud base to cloud top. Ice when present was typically spread throughout the cloud vertically with no altitude maxima.

Several profiles through the cloud layers were performed during ACCACIA. From these profiles, cloud base was found to range from 100 – 2000 m (note that this range does not include profile data where low level fog over the sea-ice was present), and cloud top from 1000 – 4000m across the flights, though higher cloud was present in some cases. The cloud layers were highly variable with lifting observed in many cases; therefore, cloud base and cloud top height was highly dependent upon the location of the profile within the cloud layer. This will have contributed to the wide range of values that were detected. Cloud sampling temperature ranged from 262 – 283 K.

Mioche et al. (2017) presented data from the ASTAR, POLARCAT and SORPIC campaigns all performed in the Greenland/Norwegian Sea region close to the ACCACIA science area. They present data from spring for only single layers over open water. Combining these project data, mean cloud top and cloud base were reported as 1200 m and 750 m respectively, which were in agreement with MPACE results to the north of Alaska (where they reported cloud top at 885 – 1320 m and cloud base at 750 m, McFarquhar et al. 2007). These clouds therefore formed at higher altitude than those sampled during the



5 summer for ACCACIA, and together with the difference in season, means the temperatures of these clouds were also different.

The in-cloud flight-mean CDP concentrations and LWC reported for the 8 ACCACIA flights were between 21.7 – 132 cm⁻³ and 0.12 – 0.48 gm⁻³ respectively. Mean CDP R_e was between 6.45 and 13.3 μm. The 2D-S reported mean total concentrations between 3.6 and 56.0 cm⁻³, with a much smaller ice component (when present) of between 4.2 x 10⁻⁴ and 8.8 x 10⁻⁴ cm⁻³. These results are consistent with previous results. Results from the ACACCIA spring campaign, reported in Young et al. 2016a, showed mean CDP number concentration ranging from 30 - 180 cm⁻³ when profiling a cloud layer from over sea-ice to over the open ocean. LWC values ranged from <0.1 gm⁻³ at cloud base to ~0.4 gm⁻³ at cloud top, with corresponding mean R_e values 4 to 11 μm. Ice was present for all flights, with a typical number concentration ~1L⁻¹.

Curry et al. (1996) reported summertime Arctic stratus results from the Barrow Atmospheric Radiation Measurement (ARM) site in Alaska. Maximum droplet number concentration and LWC was reported at 500 cm⁻³ and 0.5 gm⁻³ respectively, with mean droplet radius of 2-7 μm. Shupe et al. (2001) reported FIREACE spring/summer results (see Fig. 1 for flight region) for all liquid clouds and all ice clouds, as their technique could not be applied to mixed-phase clouds. For all liquid clouds, mean droplet concentration was 54 cm⁻³, LWC was 0.7 gm⁻³ and radius was 7.4 μm. Jackson et al. (2012) reported mean LWC of 0.15 gm⁻³ for ISDAC clouds over Alaska, with a mean droplet concentration of 150 cm⁻³. MPACE results were similar with droplet number concentrations 23 – 72 cm⁻³ and LWC 0.15 – 0.19 gm⁻³, (McFarquhar et al. 2007). Mioche et al. (2017) showed that droplet sizes were small with a slight increase from cloud base to cloud top: from 10 to 15 μm. From the two summer ACCACIA flights where there were focussed profiles through a cloud deck (see Figs. 10 and 11), cloud droplets were smaller at the cloud base than reported by Mioche et al. (2017), but do show an increase in size towards cloud top. M194 shows droplets increasing from 3 to 10 μm when over the sea-ice, and from 5 to 15 μm when over the MIZ/open water, suggesting fewer CCN. M196 shows the converse, with an increase in 5 to 12 μm from cloud base to cloud top when over the ice, and from 3 to 10 μm when over the MIZ/sea-ice surface. McFarquhar et al. (2007) reported an increase in droplet size from 14 μm at cloud base to 22 μm at cloud top for MPACE, and Jackson et al. (2012) reported an increase of 8 to 16 μm for the ISDAC campaign.

Mean ice crystal concentrations from Mioche et al. (2017), MPACE and ISDAC were reported as 3 L⁻¹, 1.6 – 5.6 L⁻¹ and 0.27 – 1 L⁻¹ respectively, with corresponding IWC reported as 0.01 – 0.035 gm⁻³, 0.006 – 0.025 gm⁻³ and 0.02 gm⁻³ respectively. None of these projects reported a consistent relationship of ice crystal concentration with altitude, indicating that the ACCACIA results are consistent with previous projects both in the same area, and further afield.

Three of the eight summer ACCACIA flights were found to sample liquid only clouds. For the remaining five, the clouds consisted predominantly of supercooled droplets, with some mixed-phase regions, and the occasional pocket of almost 100% ice. Observed ice crystal habits during summer ACCACIA varied from large irregular, stellar and columnar crystals. Rimed



5 crystals were also noted, more so near cloud base as larger ice crystals had fallen through the predominantly supercooled liquid cloud.

Model simulations typically represent ice by assuming spheres, which has an impact on the calculated ice densities, sizes and growth rates. Some models are able to apply habit information, and as such, ice habit information from this region is of interest.

10 **4.2 Lifting and thickening of cloud layers**

Where the flight track allowed the cloud microphysics to be investigated as the surface characteristics changed from sea-ice to open water, the cloud layer was observed to be thicker over open water, with higher cloud base and cloud top than over sea-ice. We have presented two cases in this paper where this can be seen (flights M194 and M196, Figs. 10 and 11 respectively). These results support the findings presented in Young et al. (2016a) which describes a case study from the
15 spring ACCACIA campaign, where cloud base and cloud top height increased from 300 m to 750 and from 650 m to 1500 m, respectively, as the aircraft sampled a cloud layer over the sea-ice to over the open ocean.

The cloud layer in M194 was at a higher altitude and shallower than the one sampled during M196. The cloud layer sampled during M194 may have been influenced by the small high pressure system to the WSW of Svalbard, with the associated large scale subsidence potentially resulting in strong downdraughts keeping the cloud top at a fairly consistent altitude
20 (Young et al. 2018). Conversely, M196 is more influenced by the surrounding low pressure, which would have an associated large scale ascent of air, resulting in the increased lift noted in the M196 cloud layer compared to the M194 cloud layer.

4.3 Glaciated pockets

When ice was detected by the 2D-S during the summer ACCACIA campaign, for the majority of the time, it was within a mixed-phase region where the cloud consisted of almost 100% supercooled water droplets. However, on occasion, it was
25 noted that the phase of the cloud particles rapidly switched from being almost 100% droplets to almost 100% ice particles. When this occurred, the ice crystal habit was predominantly columns, typical of that temperature range, but in numbers enhanced above expected ice nucleation particle concentrations, and so are indicative of secondary ice production, likely through the Hallett-Mossop process as previously reported in Lloyd et al. 2015.

4.4 Potential Sources of aerosol/IN for this project

30 Previous studies of Arctic aerosol have shown that the sources of aerosol can vary throughout the year (e.g. Sand et al 2017, Willis et al 2016). Here we have used HYSPLIT back trajectories to determine potential sources of the aerosol particles detected during out of cloud runs. This method poses a problem when runs are performed at low altitude (such as under-cloud runs) where the back trajectory often quickly intersects with the ground, beyond which the rest of the back trajectory is



- 5 not valid. We can, however, discount shipping as a source of aerosol for most of this project as there was no shipping during this time in the vicinity of Svalbard. During flights M197 and M198 the Twin Otter flew close to the JCR research vessel for a short section of the flight only. Whilst data from the JCR revealed a potential marine biogenic source of IN particles (Wilson et al. 2015), the general sea-surface conditions in the area the aircraft sampled during ACCACIA were calm, or the aircraft was over the sea-ice.
- 10 For five out of the eight flights, the Grimm detected higher aerosol levels during the high altitude SLR compared to the low SLR, indicating potential long-range transport of aerosol into the science region. Based on the trajectories shown in Fig. 5, local sources for ice nucleating particles (INP) during ACCACIA may include lofting of dust from Greenland and Iceland where the ground is partly ice-free during the summer months (e.g. Bullard et al. 2016). In addition, boreal burning in the region, or from afar, could also provide a source of IMP (e.g. Umo et al 2015). Long range transport could also have brought
- 15 Saharan dust to the region (e.g. Breider et al, 2014), and this was seen during the Spring campaign of the ACCACIA project (Young et al. 2016b), though the temperature of the clouds reported here did not go below -12 °C and so any dust particle present would likely not act as INP.

A recent paper (Dall'Osto et al 2017) has shown from data collected on Svalbard that Arctic sea ice melt leads to new particle formation as favourable conditions create particles that reach CCN sizes via secondary gas to particle nucleation and growth mechanisms. Burkart et al. (2017) also showed similar results in the Canadian Arctic. We cannot confirm the presence of such nucleation events during ACCACIA with our data set, but observations of high CPC concentrations on

20 some of the lower level runs could be an indication that these processes were relevant at the time.

As well as some previous Arctic studies showing the discrepancies in ice number and INP numbers by secondary ice formation (e.g. Lloyd et al. 2015), others have also suggested that INP recycling may be an active process in Arctic MPCs

25 (e.g. Solomon et al 2015)

5. Conclusion

In-situ aircraft observations of aerosol properties and cloud microphysics have been presented from the summertime ACCACIA project conducted in the Svalbard region during July 2013. Data from eight flights are presented. A range of cloud properties were sampled. Clouds were found to be predominantly supercooled water clouds, with small amounts of ice

30 present in 75% of flights. Several aspects of these clouds are discussed and compared to previous projects performed both in the European Arctic and elsewhere in the region; numbers are generally found to be in agreement. Data presented in this paper are available to the atmospheric science community for future data comparison or parameterisation development work.

The main conclusions of this study are as follows:



- 5
- The range of cloud microphysics parameters measured for the summertime ACCACIA project were found to be consistent with previous Arctic studies: mean CDP droplet number concentration ranged from 21.7 – 132 cm⁻³, mean CDP LWC ranged from 0.12 – 0.48 gm⁻³, mean CDP R_e ranged from 6.45 – 13.3 μm. Mean 2D-S total number concentrations ranged from 3.6 – 56.0 cm⁻³, with 2D-S ice concentrations (when present), ranging from 0.42 – 0.88 L⁻¹. Clouds were sampled across the temperature range 262 – 283 K.
- 10
- Flight-mean GRIMM below and above cloud concentrations ranged from 0.25 – 4.47 cm⁻³ and 1.29 – 21.9 cm⁻³ respectively. Mean CPC concentrations ranged from 48 – 2013 cm⁻³ and from 68.9 – 287 cm⁻³ below and above cloud respectively.
 - When cloud layers extended from over the sea-ice to over the open water, the layers were observed lift and thicken over open water compared to over sea-ice, with a smooth transition, in agreement with the springtime ACCACIA case study presented by Young et al. (2016a).
- 15
- Cloud droplet diameter was found to increase from the bottom to the top of cloud layers, increasing from 3-5 μm to 10-15 μm through clouds 200 to 600 m deep. These values are smaller than reported in other studies, particularly those studies conducted to the North of Alaska and Canada.
 - When ice was present, there was found to be no consistent relationship of ice crystal number concentration with altitude.
- 20
- Ice habits detected included irregular, stellar, and columns. Columns in particular were noted during occasional pockets of 100% ice
 - The exact sources of CCN/INP have not been determined here, though analysis of back trajectories suggests potential sources include: boreal burning in the surrounding region; summertime exposed surface; new particle formation from recent sea-ice melt; or long-range transport from Eurasia.
- 25
- These results suggest that there are generally a small number of INP present that are active at the cloud top temperatures observed. However, intermittently there are sufficient IN to initiate secondary ice processes which then dominate the glaciation process, sometimes producing a totally glaciated cloud in small pockets. This is expected to play a critical role in the water budget of the cloud by increasing the efficiency of the precipitation processes via the ice phase, and hence the lifetime of the cloud locally.
- 30

6. Data availability

35 Processed data from the ACCACIA campaign are archived on the NCAS British Atmospheric Data Centre as British Antarctic Survey (2014): British Antarctic Survey Twin Otter aircraft Meteorological Airborne Science INstrumentation (MASIN) core data for the Aerosol Cloud Coupling and Climate Interactions in the Arctic (ACCACIA) project. NCAS British Atmospheric Data Centre, 2018. doi:10.5285/0844186db1ba9e20319a2560f8d61651. Satellite data are available



- 5 from NEODAAS NERC Satellite Receiving Station, Dundee University, UK (<http://www.sat.dundee.ac.uk>). Raw cloud and aerosol data are archived at the University of Manchester and BAS, and are available on request.

7. APPENDIX I:

Table A1: Instrument acronyms for instruments listed in Table 1

Probe	Full Name	Particle Size range
2DC	2 Dimensional Cloud Probe	25 – 800 μm
2D-S	2 Dimensional Stereo Probe	10 – 1280 μm
2DP	2 Dimensional Precipitation Probe	200 – 6400 μm
CAPS	Cloud Aerosol and Precipitation Spectrometer	See: CAS, CIP, HW
CAS	Cloud Aerosol Spectrometer	0.5 – 50 μm
CCP	Cloud Combination probe	25 – 1500 μm
CDP	Cloud Droplet Probe	3 – 50 μm
CIP	Cloud Imaging Probe	CIP-15: 15 – 960 μm , CIP-100: 100 – 6400 μm
CPI	Cloud Particle Imager	15 – 2500 μm
FSSP	Forward Scattering Spectrometer Probe	FSSP-100: 0.5 – 47 μm
HALOHolo	Holographic cloud probe	6 μm – 1 cm
HVPS	High Volume Precipitation Spectrometer	150 μm – 1.92 cm
HW	Hot wire probe	(bulk liquid water content)
Nevzorov	Nevzorov liquid and total water content Probe	(bulk liquid and total condensed water content)
PIP	Precipitation Imaging Probe	100 – 6400 μm
PN	Polar Nephelometer	(scattering)
SID3	Small Ice Detector 3	5 – 100 μm

10 8. Supplement links

To be provided

9. Acknowledgements

- 15 This work was funded by NERC grant NE/I028653/1 and NE/I028696/1. The authors thank the UK Met Office for forecast products and Norwegian Met Office for daily pressure charts used during flight planning. Thanks to the MASIN pilot, Al Howland, for the successful operation of the aircraft during ACCACIA. Special thanks to Paul Lawson and SPEC Inc. for their help and support with the provisions of the 2D-S probe used on the Twin Otter. We would like to thank Jonathan Crosier (University of Manchester) for help with data processing using OASIS software and discussions.

References

- ACIA, Arctic Climate Impact Assessment, Cambridge University Press, Cambridge, 1042 pp., 2005.
- 20 Allan, J. D., Williams, P. I., Najera, J., Whitehead, J. D., Flynn, M. J., Taylor, J. W., Liu, D., Darbyshire, E., Carpenter, L. J., Chance, R., Andrews, S. J., Hackenberg, S. C., and McFiggans, G.: Iodine observed in new particle formation events in the Arctic atmosphere during ACCACIA, Atmos Chem Phys, 15, 5599-5609, 10.5194/acp-15-5599-2015, 2015.



- 5 Baumgardner, D., Jonsson, H., Dawson, W., O'Connor, D., and Newton, R.: The cloud, aerosol and precipitation spectrometer: a new instrument for cloud investigations, *Atmos Res*, 59, 251-264, Doi 10.1016/S0169-8095(01)00119-3, 2001.
- Bierwirth, E., Ehrlich, A., Wendisch, M., Gayet, J. F., Gourbeyre, C., Dupuy, R., Herber, A., Neuber, R., and Lampert, A.: Optical thickness and effective radius of Arctic boundary-layer clouds retrieved from airborne nadir and imaging spectrometry, *Atmos Meas Tech*, 6, 1189-1200, 10.5194/amt-6-1189-2013, 2013.
- 10 Breider, T. J., Mickley, L. J., Jacob, D. J., Wang, Q. Q., Fisher, J. A., Chang, R. Y. W., and Alexander, B.: Annual distributions and sources of Arctic aerosol components, aerosol optical depth, and aerosol absorption, *J Geophys Res-Atmos*, 119, 4107-4124, 10.1002/2013jd020996, 2014.
- Brock, C. A., Cozic, J., Bahreini, R., Froyd, K. D., Middlebrook, A. M., McComiskey, A., Brioude, J., Cooper, O. R., Stohl, A., Aikin, K. C., de Gouw, J. A., Fahey, D. W., Ferrare, R. A., Gao, R. S., Gore, W., Holloway, J. S., Hubler, G., Jefferson, A., Lack, D. A., Lance, S., Moore, R. H., Murphy, D. M., Nenes, A., Novelli, P. C., Nowak, J. B., Ogren, J. A., Peischl, J., Pierce, R. B., Pilewskie, P., Quinn, P. K., Ryerson, T. B., Schmidt, K. S., Schwarz, J. P., Sodemann, H., Spackman, J. R., Stark, H., Thomson, D. S., Thornberry, T., Veres, P., Watts, L. A., Warneke, C., and Wollny, A. G.: Characteristics, sources, and transport of aerosols measured in spring 2008 during the aerosol, radiation, and cloud processes affecting Arctic Climate (ARCPAC) Project, *Atmos Chem Phys*, 11, 2423-2453, 10.5194/acp-11-2423-2011, 2011.
- 20 Brown, P. R. A., and Francis, P. N.: Improved Measurements of the Ice Water-Content in Cirrus Using a Total-Water Probe, *J Atmos Ocean Tech*, 12, 410-414, Doi 10.1175/1520-0426(1995)012<0410:Imotiw>2.0.Co;2, 1995.
- Bullard, J. E., Baddock, M., Bradwell, T., Crusius, J., Darlington, E., Gaiero, D., Gasso, S., Gisladottir, G., Hodgkins, R., McCulloch, R., McKenna-Neuman, C., Mockford, T., Stewart, H., and Thorsteinsson, T.: High-latitude dust in the Earth system, *Rev Geophys*, 54, 447-485, 10.1002/2016rg000518, 2016.
- 25 Burkart, J., Willis, M. D., Bozem, H., Thomas, J. L., Law, K., Hoor, P., Aliabadi, A. A., Kollner, F., Schneiders, J., Herber, A., Abbatt, J. P. D., and Leaitch, W. R.: Summertime observations of elevated levels of ultrafine particles in the high Arctic marine boundary layer, *Atmos Chem Phys*, 17, 5515-5535, 10.5194/acp-17-5515-2017, 2017.
- Crosier, J., Bower, K. N., Choulaton, T. W., Westbrook, C. D., Connolly, P. J., Cui, Z. Q., Crawford, I. P., Capes, G. L., Coe, H., Dorsey, J. R., Williams, P. I., Illingworth, A. J., Gallagher, M. W., and Blyth, A. M.: Observations of ice multiplication in a weakly convective cell embedded in supercooled mid-level stratus, *Atmos Chem Phys*, 11, 257-273, 10.5194/acp-11-257-2011, 2011.
- 30 Crosier, J., Choulaton, T. W., Westbrook, C. D., Blyth, A. M., Bower, K. N., Connolly, P. J., Dearden, C., Gallagher, M. W., Cui, Z., and Nicol, J. C.: Microphysical properties of cold frontal rainbands, *Q J Roy Meteor Soc*, 140, 1257-1268, 10.1002/qj.2206, 2014.
- 35 Curry, J. A., Rossow, W. B., Randall, D., and Schramm, J. L.: Overview of Arctic cloud and radiation characteristics, *J Climate*, 9, 1731-1764, Doi 10.1175/1520-0442(1996)009<1731:Ooacar>2.0.Co;2, 1996.
- Dall'Osto, M., Beddows, D. C. S., Tunved, P., Krejci, R., Strom, J., Hansson, H. C., Yoon, Y. J., Park, K. T., Becagli, S., Udisti, R., Onasch, T., O'Dowd, C. D., Simo, R., and Harrison, R. M.: Arctic sea ice melt leads to atmospheric new particle formation, *Sci Rep-Uk*, 7, 10.1038/s41598-017-03328-1, 2017.
- 40



- 5 Dee, D. P., Uppala, S. M., Simmons, A. J., Berrisford, P., Poli, P., Kobayashi, S., Andrae, U., Balmaseda, M. A., Balsamo, G., Bauer, P., Bechtold, P., Beljaars, A. C. M., van de Berg, L., Bidlot, J., Bormann, N., Delsol, C., Dragani, R., Fuentes, M., Geer, A. J., Haimberger, L., Healy, S. B., Hersbach, H., Holm, E. V., Isaksen, L., Kallberg, P., Kohler, M., Matricardi, M., McNally, A. P., Monge-Sanz, B. M., Morcrette, J. J., Park, B. K., Peubey, C., de Rosnay, P., Tavolato, C., Thepaut, J. N., and Vitart, F.: The ERA-Interim reanalysis: configuration and performance of the data assimilation system, *Q J Roy Meteor Soc*, 137, 553-597, 10.1002/qj.828, 2011.
- 10 Draxler, R. R., and Hess, G. D.: An overview of the Hysplit_4 modeling system for trajectories, dispersion, and deposition. , *Aust Met Mag*, 295 - 308, 1998.
- Fiedler, E. K., Lachlan-Cope, T. A., Renfrew, I. A., and King, J. C.: Convective heat transfer over thin ice covered coastal polynyas, *J Geophys Res-Oceans*, 115, 10.1029/2009jc005797, 2010.
- 15 Fleming, Z. L., Monks, P. S., and Manning, A. J.: Review: Untangling the influence of air-mass history in interpreting observed atmospheric composition, *Atmos Res*, 104, 1-39, 10.1016/j.atmosres.2011.09.009, 2012.
- Garman, K. E., Hill, K. A., Wyss, P., Carlsen, M., Zimmerman, J. R., Stirm, B. H., Carney, T. Q., Santini, R., and Shepson, P. B.: An airborne and wind tunnel evaluation of a wind turbulence measurement system for aircraft-based flux measurements, *J Atmos Ocean Tech*, 23, 1696-1708, Doi 10.1175/Jtech1940.1, 2006.
- 20 Gayet, J. F., Treffeisen, R., Helbig, A., Bareiss, J., Matsuki, A., Herber, A., and Schwarzenboeck, A.: On the onset of the ice phase in boundary layer Arctic clouds, *J Geophys Res-Atmos*, 114, 10.1029/2008jd011348, 2009.
- Glen, A., and Brooks, S. D.: A new method for measuring optical scattering properties of atmospherically relevant dusts using the Cloud and Aerosol Spectrometer with Polarization (CASPOL), *Atmos Chem Phys*, 13, 1345-1356, 10.5194/acp-13-1345-2013, 2013.
- 25 Hallett, J., and Mossop, S. C.: Production of Secondary Ice Particles during Riming Process, *Nature*, 249, 26-28, DOI 10.1038/249026a0, 1974.
- Jackson, R. C., McFarquhar, G. M., Korolev, A. V., Earle, M. E., Liu, P. S. K., Lawson, R. P., Brooks, S., Wolde, M., Laskin, A., and Freer, M.: The dependence of ice microphysics on aerosol concentration in arctic mixed-phase stratus clouds during ISDAC and M-PACE, *J Geophys Res-Atmos*, 117, 10.1029/2012jd017668, 2012.
- 30 Jacob, D. J., Crawford, J. H., Maring, H., Clarke, A. D., Dibb, J. E., Emmons, L. K., Ferrare, R. A., Hostetler, C. A., Russell, P. B., Singh, H. B., Thompson, A. M., Shaw, G. E., McCauley, E., Pederson, J. R., and Fisher, J. A.: The Arctic Research of the Composition of the Troposphere from Aircraft and Satellites (ARCTAS) mission: design, execution, and first results, *Atmos Chem Phys*, 10, 5191-5212, 10.5194/acp-10-5191-2010, 2010.
- 35 Kay, J. E., and Gettelman, A.: Cloud influence on and response to seasonal Arctic sea ice loss, *J Geophys Res-Atmos*, 114, Artn D18204 10.1029/2009jd011773, 2009.
- King, J. C., Lachlan-Cope, T. A., Ladkin, R. S., and Weiss, A.: Airborne measurements in the stable boundary layer over the Larsen Ice Shelf, Antarctica, *Bound-Lay Meteorol*, 127, 413-428, 10.1007/s10546-008-9271-4, 2008.



- 5 Korolev, A. V., Emery, E. F., Strapp, J. W., Cober, S. G., Isaac, G. A., Wasey, M., and Marcotte, D.: Small Ice Particles in Tropospheric Clouds: Fact or Artifact? Airborne Icing Instrumentation Evaluation Experiment, *B Am Meteorol Soc*, 92, 967-973, 10.1175/2010bams3141.1, 2011.
- Korolev, A. V., Emery, E. F., Strapp, J. W., Cober, S. G., and Isaac, G. A.: Quantification of the Effects of Shattering on Airborne Ice Particle Measurements, *J Atmos Ocean Tech*, 30, 2527-2553, 10.1175/Jtech-D-13-00115.1, 2013.
- 10 Lampert, A., Ritter, C., Hoffmann, A., Gayet, J. F., Mioche, G., Ehrlich, A., Dornbrack, A., Wendisch, M., and Shiobara, M.: Lidar characterization of the Arctic atmosphere during ASTAR 2007: four cases studies of boundary layer, mixed-phase and multi-layer clouds, *Atmos Chem Phys*, 10, 2847-2866, DOI 10.5194/acp-10-2847-2010, 2010.
- Lance, S., Brock, C. A., Rogers, D., and Gordon, J. A.: Water droplet calibration of the Cloud Droplet Probe (CDP) and in-flight performance in liquid, ice and mixed-phase clouds during ARCPAC, *Atmos Meas Tech*, 3, 1683-1706, 10.5194/amt-3-1683-2010, 2010.
- 15 Lawson, R. P., Baker, B. A., Schmitt, C. G., and Jensen, T. L.: An overview of microphysical properties of Arctic clouds observed in May and July 1998 during FIRE ACE, *J Geophys Res-Atmos*, 106, 14989-15014, Doi 10.1029/2000jd900789, 2001.
- Lawson, R. P., O'Connor, D., Zmarzly, P., Weaver, K., Baker, B., Mo, Q. X., and Jonsson, H.: The 2D-S (Stereo) probe: Design and preliminary tests of a new airborne, high-speed, high-resolution particle Imaging probe, *J Atmos Ocean Tech*, 23, 1462-1477, Doi 10.1175/Jtech1927.1, 2006.
- 20 Lloyd, G., Choullarton, T. W., Bower, K. N., Crosier, J., Jones, H., Dorsey, J. R., Gallagher, M. W., Connolly, P., Kirchgaessner, A. C. R., and Lachlan-Cope, T.: Observations and comparisons of cloud microphysical properties in spring and summertime Arctic stratocumulus clouds during the ACCACIA campaign, *Atmos Chem Phys*, 15, 3719-3737, 10.5194/acp-15-3719-2015, 2015.
- 25 McFarquhar, G. M., Zhang, G., Poellot, M. R., Kok, G. L., McCoy, R., Tooman, T., Fridlind, A., and Heymsfield, A. J.: Ice properties of single-layer stratocumulus during the Mixed-Phase Arctic Cloud Experiment: 1. Observations, *J Geophys Res-Atmos*, 112, Artn D24201 10.1029/2007jd008633, 2007.
- McFarquhar, G. M., Ghan, S., Verlinde, J., Korolev, A., Strapp, J. W., Schmid, B., Tomlinson, J. M., Wolde, M., Brooks, S. D., Cziczo, D., Dubey, M. K., Fan, J. W., Flynn, C., Gultepe, I., Hubbe, J., Gilles, M. K., Laskin, A., Lawson, P., Leitch, W. R., Liu, P., Liu, X. H., Lubin, D., Mazzoleni, C., Macdonald, A. M., Moffet, R. C., Morrison, H., Ovchinnikov, M., Shupe, M. D., Turner, D. D., Xie, S. C., Zelenyuk, A., Bae, K., Freer, M., and Glen, A.: INDIRECT AND SEMI-DIRECT AEROSOL CAMPAIGN The Impact of Arctic Aerosols on Clouds, *B Am Meteorol Soc*, 92, 183-201, 10.1175/2010bams2935.1, 2011.
- 30 Mioche, G., Jourdan, O., Ceccaldi, M., and Delanoe, J.: Variability of mixed-phase clouds in the Arctic with a focus on the Svalbard region: a study based on spaceborne active remote sensing, *Atmos Chem Phys*, 15, 2445-2461, 10.5194/acp-15-2445-2015, 2015.
- Mioche, G., Jourdan, O., Delanoe, J., Goubeyre, C., Febvre, G., Dupuy, R., Monier, M., Szczap, F., Schwarzenboeck, A., and Gayet, J. F.: Vertical distribution of microphysical properties of Arctic springtime low-level mixed-phase clouds over the Greenland and Norwegian seas, *Atmos Chem Phys*, 17, 12845-12869, 10.5194/acp-17-12845-2017, 2017.
- 40



- 5 Mioche, G., and Jourdan, O.: Spaceborne Remote Sensing and Airborne In Situ Observations of Arctic Mixed-Phase Clouds, *Mixed-Phase Clouds: Observations and Modeling*, 121-150, [10.1016/B978-0-12-810549-8.00006-4](https://doi.org/10.1016/B978-0-12-810549-8.00006-4), 2018.
- Morrison, H., de Boer, G., Feingold, G., Harrington, J., Shupe, M. D., and Sulia, K.: Resilience of persistent Arctic mixed-phase clouds, *Nat Geosci*, 5, 11-17, [10.1038/Ngeo1332](https://doi.org/10.1038/Ngeo1332), 2012.
- 10 Peng, G., Meier, W. N., Scott, D. J., and Savoie, M. H.: A long-term and reproducible passive microwave sea ice concentration data record for climate studies and monitoring, *Earth Syst Sci Data*, 5, 311-318, [10.5194/essd-5-311-2013](https://doi.org/10.5194/essd-5-311-2013), 2013.
- Rossow, W. B., and Garder, L. C.: Validation of Isccp Cloud Detections, *J Climate*, 6, 2370-2393, [Doi 10.1175/1520-0442\(1993\)006<2370:Voicd>2.0.Co;2](https://doi.org/10.1175/1520-0442(1993)006<2370:Voicd>2.0.Co;2), 1993.
- 15 Sand, M., Samset, B. H., Balkanski, Y., Bauer, S., Bellouin, N., Berntsen, T. K., Bian, H., Chin, M., Diehl, T., Easter, R., Ghan, S. J., Iversen, T., Kirkevåg, A., Lamarque, J. F., Lin, G. X., Liu, X. H., Luo, G., Myhre, G., van Noije, T., Penner, J. E., Schulz, M., Seland, O., Skeie, R. B., Stier, P., Takemura, T., Tsigaridis, K., Yu, F. Q., Zhang, K., and Zhang, H.: Aerosols at the poles: an AeroCom Phase II multi-model evaluation, *Atmos Chem Phys*, 17, 12197-12218, [10.5194/acp-17-12197-2017](https://doi.org/10.5194/acp-17-12197-2017), 2017.
- 20 Schafer, M., Bierwirth, E., Ehrlich, A., Jakel, E., and Wendisch, M.: Airborne observations and simulations of three-dimensional radiative interactions between Arctic boundary layer clouds and ice floes, *Atmos Chem Phys*, 15, 8147-8163, [10.5194/acp-15-8147-2015](https://doi.org/10.5194/acp-15-8147-2015), 2015.
- Sedlar, J., Tjernstrom, M., Mauritsen, T., Shupe, M. D., Brooks, I. M., Persson, P. O. G., Birch, C. E., Leck, C., Sirevaag, A., and Nicolaus, M.: A transitioning Arctic surface energy budget: the impacts of solar zenith angle, surface albedo and cloud radiative forcing, *Clim Dynam*, 37, 1643-1660, [10.1007/s00382-010-0937-5](https://doi.org/10.1007/s00382-010-0937-5), 2011.
- 25 Shupe, M. D., Walden, V. P., Eloranta, E., Uttal, T., Campbell, J. R., Starkweather, S. M., and Shiobara, M.: Clouds at Arctic Atmospheric Observatories. Part I: Occurrence and Macrophysical Properties, *J Appl Meteorol Clim*, 50, 626-644, [10.1175/2010jamc2467.1](https://doi.org/10.1175/2010jamc2467.1), 2011.
- Solomon, A., Feingold, G., and Shupe, M. D.: The role of ice nuclei recycling in the maintenance of cloud ice in Arctic mixed-phase stratocumulus, *Atmos Chem Phys*, 15, 10631-10643, [10.5194/acp-15-10631-2015](https://doi.org/10.5194/acp-15-10631-2015), 2015.
- 30 Tan, I., Storelvmo, T., and Zelinka, M. D.: Observational constraints on mixed-phase clouds imply higher climate sensitivity, *Science*, 352, 224-227, [10.1126/science.aad5300](https://doi.org/10.1126/science.aad5300), 2016.
- Taylor, J. W., Choullarton, T. W., Blyth, A. M., Liu, Z., Bower, K. N., Crosier, J., Gallagher, M. W., Williams, P. I., Dorsey, J. R., Flynn, M. J., Bennett, L. J., Huang, Y., French, J., Korolev, A., and Brown, P. R. A.: Observations of cloud microphysics and ice formation during COPE, *Atmos Chem Phys*, 16, 799-826, [10.5194/acp-16-799-2016](https://doi.org/10.5194/acp-16-799-2016), 2016.
- 35 Tjernstrom, M., Leck, C., Persson, P. O. G., Jensen, M. L., Oncley, S. P., and Targino, A.: The summertime Arctic atmosphere - Meteorological measurements during the Arctic Ocean experiment 2001, *B Am Meteorol Soc*, 85, 1305-1321, [10.1175/Bams-85-9-1305](https://doi.org/10.1175/Bams-85-9-1305), 2004.



- 5 Umo, N. S., Murray, B. J., Baeza-Romero, M. T., Jones, J. M., Lea-Langton, A. R., Malkin, T. L., O'Sullivan, D., Neve, L., Plane, J. M. C., and Williams, A.: Ice nucleation by combustion ash particles at conditions relevant to mixed-phase clouds, *Atmos Chem Phys*, 15, 5195-5210, [10.5194/acp-15-5195-2015](https://doi.org/10.5194/acp-15-5195-2015), 2015.
- Uttal, T., Curry, J. A., McPhee, M. G., Perovich, D. K., Moritz, R. E., Maslanik, J. A., Guest, P. S., Stern, H. L., Moore, J. A., Turenne, R., Heiberg, A., Serreze, M. C., Wylie, D. P., Persson, O. G., Paulson, C. A., Halle, C., Morison, J. H.,
10 Wheeler, P. A., Makshtas, A., Welch, H., Shupe, M. D., Intrieri, J. M., Stamnes, K., Lindsey, R. W., Pinkel, R., Pegau, W. S., Stanton, T. P., and Grenfeld, T. C.: Surface heat budget of the Arctic Ocean, *B Am Meteorol Soc*, 83, 255-275, [Doi 10.1175/1520-0477\(2002\)083<0255:Shbota>2.3.Co;2](https://doi.org/10.1175/1520-0477(2002)083<0255:Shbota>2.3.Co;2), 2002.
- Verlinde, J., Harrington, J. Y., McFarquhar, G. M., Yannuzzi, V. T., Avramov, A., Greenberg, S., Johnson, N., Zhang, G., Poellot, M. R., Mather, J. H., Turner, D. D., Eloranta, E. W., Zak, B. D., Prenni, A. J., Daniel, J. S., Kok, G. L., Tobin, D. C.,
15 Holz, R., Sassen, K., Spangenberg, D., Minnis, P., Tooman, T. P., Ivey, M. D., Richardson, S. J., Bahrmann, C. P., Shupe, M., DeMott, P. J., Heymsfield, A. J., and Schofield, R.: The mixed-phase Arctic cloud experiment, *B Am Meteorol Soc*, 88, 205-221, [10.1175/Bams-88-2-205](https://doi.org/10.1175/Bams-88-2-205), 2007.
- Willis, M. D., Burkart, J., Thomas, J. L., Kollner, F., Schneider, J., Bozem, H., Hoor, P. M., Aliabadi, A. A., Schulz, H., Herber, A. B., Leaitch, W. R., and Abbatt, J. P. D.: Growth of nucleation mode particles in the summertime Arctic: a case
20 study, *Atmos Chem Phys*, 16, 7663-7679, [10.5194/acp-16-7663-2016](https://doi.org/10.5194/acp-16-7663-2016), 2016.
- Wilson, T. W., Ladino, L. A., Alpert, P. A., Breckels, M. N., Brooks, I. M., Browse, J., Burrows, S. M., Carslaw, K. S., Huffman, J. A., Judd, C., Kilhau, W. P., Mason, R. H., McFiggans, G., Miller, L. A., Najera, J. J., Polishchuk, E., Rae, S., Schiller, C. L., Si, M., Temprado, J. V., Whale, T. F., Wong, J. P. S., Wurl, O., Yakobi-Hancock, J. D., Abbatt, J. P. D.,
25 Aller, J. Y., Bertram, A. K., Knopf, D. A., and Murray, B. J.: A marine biogenic source of atmospheric ice-nucleating particles, *Nature*, 525, 234-+, [10.1038/nature14986](https://doi.org/10.1038/nature14986), 2015.
- Young, G., Jones, H. M., Choulaton, T., Crosier, J., Bower, K. N., Gallagher, M., Davies, R. S., Renfrew, I. A., Elvidge, A. D., Darbyshire, E., Marengo, F., Brown, P. R. A., Ricketts, H. M. A., Connolly, P. J., Lloyd, G., Williams, P. I., Allan, J. D., Taylor, J. W., Liu, D. T., and Flynn, M. J.: Observed microphysical changes in Arctic mixed-phase clouds when transitioning from sea ice to open ocean, *Atmos Chem Phys*, 16, 13945-13967, [10.5194/acp-16-13945-2016](https://doi.org/10.5194/acp-16-13945-2016), 2016a.
- 30 Young, G., Jones, H. M., Darbyshire, E., Baustian, K. J., McQuaid, J. B., Bower, K. N., Connolly, P. J., Gallagher, M. W., and Choulaton, T. W.: Size-segregated compositional analysis of aerosol particles collected in the European Arctic during the ACCACIA campaign, *Atmos Chem Phys*, 16, 4063-4079, 2016b.
- Young, G., Connolly, P. J., Dearden, C., and Choulaton, T. W.: Relating large-scale subsidence to convection development in Arctic mixed-phase marine stratocumulus, *Atmos Chem Phys*, 18, 1475-1494, [10.5194/acp-18-1475-2018](https://doi.org/10.5194/acp-18-1475-2018), 2018.



5 **Table 1: Previous Arctic projects with in-situ cloud measurements. Cloud instrumentation is listed in abbreviated form for brevity; see Appendix I for full details. This table highlights the range of regions sampled during different seasons often using different instrumentation or set up. Data comparison between different campaigns should be carried out with care, with consideration given to instrument and software development over time. A similar table can be found in Mioche and Jourdan (2018).**

Project	Location	Date	Cloud instrumentation	Aircraft	Reference
FIREACE I & II First International Satellite Cloud Climatology Project Regional Experiment Arctic Clouds Experiment	Alaska	April and July 1998	CPI FSSP 2DC	C-130	Lawson et al. 2001
M-PACE Mixed-Phase Arctic Cloud Experiment	Alaska	Sept-Oct 2004	HVPS LIDAR FSSP, 2DC	Citation	Verlinde et al. 2007
ASTAR Arctic Study of Tropospheric Aerosols, clouds and Radiation experiments	Svalbard (Sea/land)	April 2007	CPI PN FSSP-100/2DC Nevzorov	Polar-2 DLR Falcon	Lampert et al. 2010
ARCTAS Arctic Research on the Composition of the Troposphere Aircraft and Satellites	Canada, Greenland, Alaska from (mostly land, sea)	April 2008 Jun /Jul 2008	Lidar	NASA DC-8 P-3B B200	Jacob et al. 2010
ARCPAC Aerosol, Radiation, and Cloud Processes affecting Arctic Climate	Canada, Alaska (mostly land)	April 2008	CDP CIP HW	NOAA WP-3D	Brock et al. 2011
ISDAC Indirect and Semi- direct Aerosol Campaign	Alaska	April 2008	Nevzorov CDP CAPS 2D-S FSSP-100 FSSP-300 2DC, 2DP	Convair-580	McFarquhar et al. 2011
SORPIC SOLar Radiation and Phase discrimination of arctic Clouds	Svalbard (Sea/land)	April/May 2010	CPI FSSP-100 PN Nevzerov	Polar-5	Bierwirth et al. 2013



VERDI	Beaufort sea	April-	SID-3	Polar 5	Schafer et al.
Vertical Distribution of	(sea, land)	May2012	CCP (CIP + CDP)		2015
Ice in Arctic Clouds			CAS-DPOL		
RACEPAC	Canada	April/May	CCP, PIP, HaloHolo, Polar 5		
Radiation-Aerosol-	(Land, sea, sea-	2014	CAPS, SID3, PN		
Cloud Experiment	in ice)				
the Arctic Circle					

5



- 5 **Table 2: Information on the ACCACIA summer flights, including the wind direction and percentage of the flight that the aircraft sampled cloud. Minimum and maximum temperatures are calculated from aircraft data in the science region only (i.e. does not include data from take-off and landing). Ice latitude edge is the latitude at which 50% ice cover was reported by NSIDC. Letters in the first column correspond to the parts of Fig. 3.**

Flight	Date	Duration (% cloud)	Prevailing winds*	Ice edge latitude	Temperature range [K]	Flight aims
M190 (a)	17/07/2013	2hr37min				Test Flight Inlet characterisation
M191 (b)	18/07/2013	5hr40min (27.3%)	From west	81N	262 - 279	Cloud flight
M192 (c)	19/07/2013	5hr11min (17.9%)	From SW	81N	268 - 283	Cloud flight
M193 (d)	22/07/2013	6hr0min (53.5%)	From SW (SE over ice)	81N	262 - 277	Cloud flight
M194 (e)	23/07/2013	4hr27min (27.4%)	From W (SW nearer Svalbard)	81.5N	262 - 275	Cloud flight
M195 (f)	25/07/2013	5hr17min (17.9%)	From SW	79N	263 - 276	Cloud flight
M196 (g)	26/07/2013	4hr28min (47.6%)	From SW	82N	270 - 277	Cloud flight
M197 (h)	29/07/2013	4hr43min (20.8%)	Strongly From SE at N end, weakly from S at S end	78.5N	270 - 280	JCR Overpass. Surface fluxes
M198 (i)	30/07/2013	5hr9min (28.6%)	From NW	79.5N	270 - 276	Cloud flight

*relative to Svalbard.



5 **Table 3: Overview of aerosol data from the summer ACCACIA flights. Mean altitude and RH are calculated over**
straight and level runs (SLRs) during cloud-free periods, and have been separated into below cloud and above cloud
layer(s) SLRs. These sample times were filtered to remove any in-cloud data points by applying a CDP liquid-water
content cut-off of 0.01 gm^{-3} . Numbers shown are mean values from at least a 5 minute period (standard deviation
 10 **shown in brackets). The GRIMM and CPC sampled through a heated inlet inside the aircraft, whereas the CAS was**
mounted on a wing-pylon and sampled ambient air.

Flight	Altitude [m]	RH [%]	GRIMM total concentration [cm^{-3}]	CPC total concentration [cm^{-3}]	CAS total concentration [cm^{-3}]	Predominant surface in flight region
M191	350m	79.4	1.14 (1.21)	175 (77)	0.10 (0.11)	Over ocean
	125m	84.3	0.77 (0.66)	261 (208)	0.48 (0.39)	
M192	3380m	82.7	5.83 (0.83)	196 (13)	0.30 (1.42)	Over ocean
	60m	92.5	2.54 (0.96)	1080 (1065)	1.45 (0.58)	Over ice edge
	100m	85.7	4.00 (1.04)	1388 (700)	1.56 (0.67)	
M193	2650m	55.0	6.93 (1.48)	204 (48)	0.24 (0.36)	Over South east coast
	60m	95.0	3.35 (0.61)	136 (11)	3.09 (0.73)	Over sea ice
	60m	88.4	3.79 (1.30)	81 (26)	3.95 (1.59)	
M194	3020m	66.9	8.10 (2.38)	226 (45)	0.25 (0.16)	Over ocean
	350m	92.1	2.6 (2.2)	48 (33)	0.15 (0.17)	Over sea ice
M195	3000m	81.1	2.8 (1.2)	287 (56)	0.11 (0.09)	Over sea ice
	200m	87.3	0.72 (0.77)	90.4 (26.1)	0.27 (0.24)	Over ice/ocean
	60m	93.7	0.66 (0.19)	154.8 (29.4)	0.29 (0.14)	Over sea ice
M196	1050m	82.9	1.29 (1.25)	68.9 (40.0)	0.10 (0.11)	Over ocean
	120m	89.6	4.47 (0.94)	294 (27)	1.19 (0.59)	Over ocean
M197	2400m	71.4	4.97 (0.57)	157 (9)	0.15 (0.10)	Over land
	210m	98.8	0.25 (0.50)	1154 (794)	0.50 (0.2)	Over sea ice
M198	2400m	33.5	21.9 (20.9)	206 (48)	2.33 (0.16)	Over ice edge
	400m	82.7	0.80 (0.86)	2013 (151)	0.06 (0.06)	Over sea ice
	310m	93.1	0.64 (0.33)	1788 (340)	0.06 (0.07)	Over sea ice



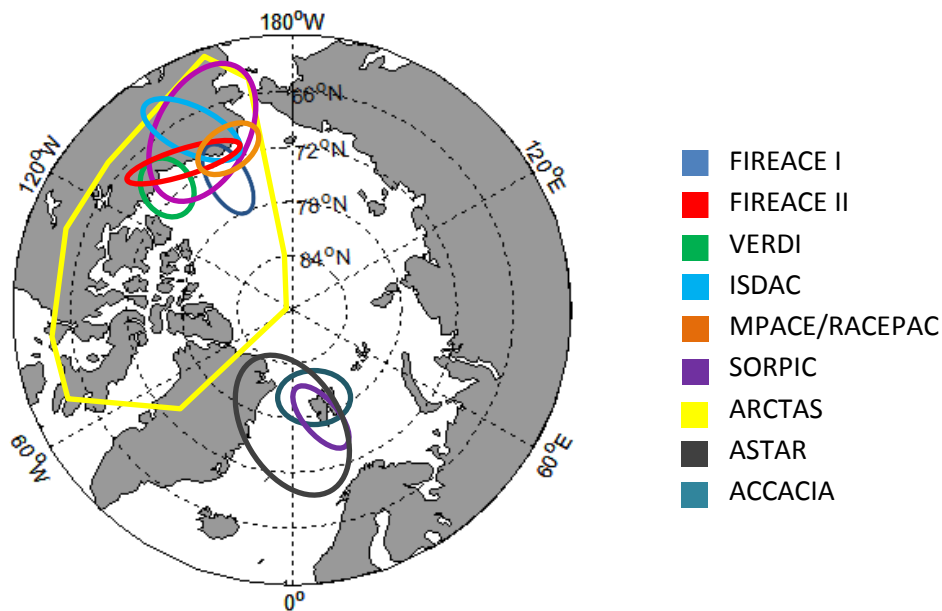
2450m	56.4	5.78 (4.31)	192 (110)	0.04 (0.05)	Over sea ice
-------	------	-------------	-----------	-------------	--------------

5



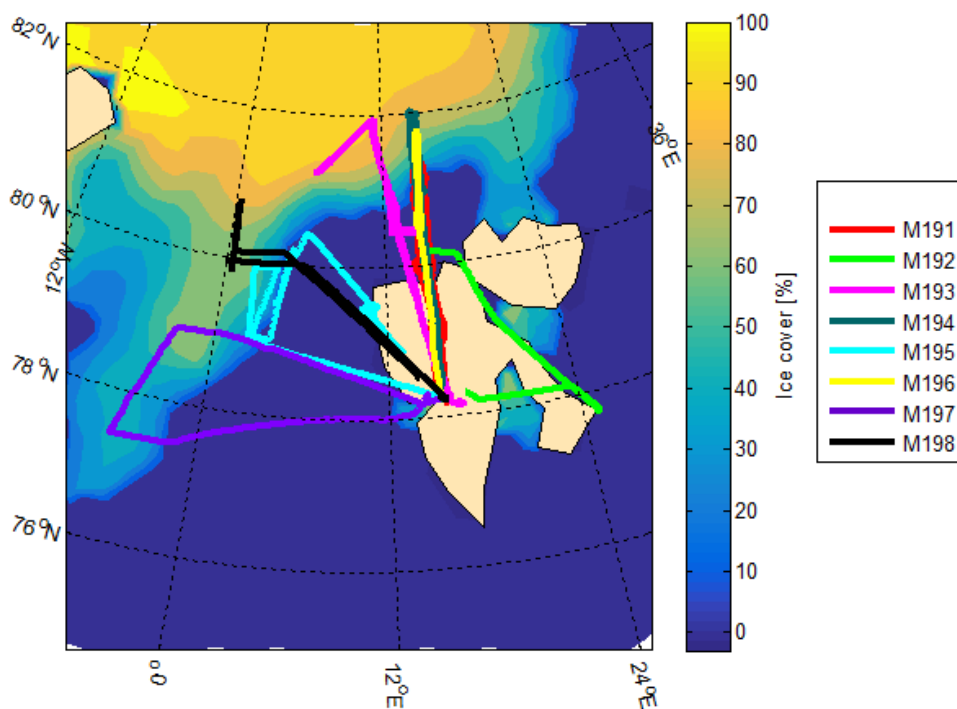
5 **Table 4: An overview of the cloud data collected during the summer ACCACIA campaign. Data have been presented**
for each flight as follows: Top row – “mean (standard deviation)”, bottom row – “(25th percentile) median (75th
percentile)”. Mean and percentile values of the number concentration, liquid water content and effective radius have
been calculated for all in-cloud times when sampling in the science area (i.e. transit excluded), when the CDP sampled
at least >0.01 gm⁻³, and the 2D-S sampled non-zero data. 2D-S total number concentration includes edge particle, 2D-
 10 **S ‘ice’ is the number concentration of particles with high irregularity.**

Flight	CDP Conc [cm ⁻³]	CDP LWC [g/m ³]	CDP R _e [μm]	2D-S Total [cm ⁻³]	2D-S ‘ice’ [cm ⁻³]
M191	132 (59) (89) 134 (172)	0.13 (0.10) (0.06) 0.11 (0.16)	6.45 (2.06) (5.24) 6.06 (7.17)	16.3 (24.3) (0.2) 5.4 (23.4)	4.6e-4 (1.4e-3) (0) 0 (2.0e-4)
M192	128 (98) (54) 99 (184)	0.21 (0.22) (0.07) 0.14 (0.29)	7.97 (2.77) (5.97) 7.69 (9.53)	25.2 (35.9) (0.1) 9.7 (38.4)	5.6e-4 (1.1e-3) (0) 1.8e-4 (5.7e-4)
M193	21.7 (19.4) (5.9) 14.8 (33.6)	0.08 (0.08) (0.03) 0.05 (0.10)	12.04 (4.74) (7.9) 11.65 (15.2)	3.6 (6.5) (0.01) 0.19 (4.8)	8.8e-4 (1.6e3) (0) 2.4e-4 (8.8e-4)
M194	57.5 (49.0) (28.6) 43.7 (59.7)	0.16 (0.12) (0.07) 0.13 (0.25)	9.77 (3.21) (6.93) 10.2 (12.3)	15.9 (17.4) (0.1) 8.2 (31.3)	5.2e-4 (1.6e-3) (0) 0 (2.0e-4)
M195	92.2 (44.2) (61.5) 88.1 (124)	0.13 (0.09) (0.06) 0.11 (0.17)	7.16 (1.70) (6.0) 7.0 (8.2)	20.6 (24.1) (0.6) 11.2 (32.3)	4.2e-4 (1.0e-3) (0) 0 (3.8e-4)
M196	118.4 (48.1) (83.7) 117 (154)	0.48 (0.27) (0.25) 0.45 (0.70)	10.2 (2.01) (8.91) 10.6 (11.7)	56.0 (47.4) (0.5) 55.8 (93.7)	No ice detected
M197	44.5 (55.3) (4.4) 11.9 (75.6)	0.20 (0.20) (0.04) 0.09 (0.39)	13.3 (4.07) (10.6) 12.5 (15.4)	13.0 (13.3) (1.35) 9.1 (22.0)	No ice detected
M198	30.7 (21.0) (13.3) 28.9 (43.8)	0.12 (0.1) (0.05) 0.1 (0.18)	11.1 (3.3) (8.5) 10.6 (13.1)	32.0 (43.2) (1.1) 4.6 (58.2)	No ice detected



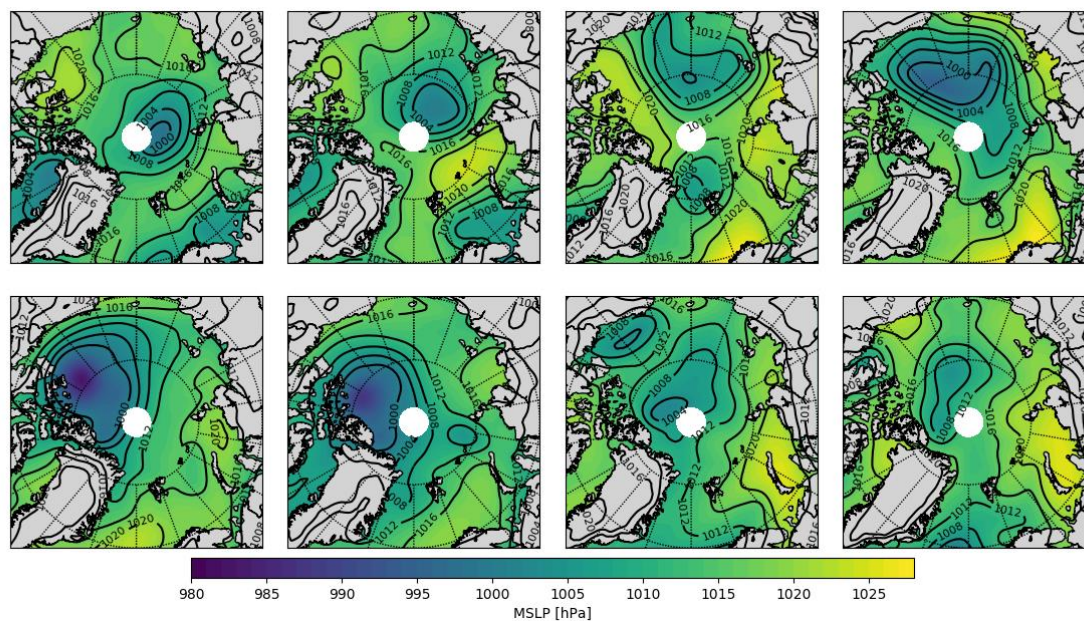
5

Figure 1: Measurement regions of some previous Arctic flight campaigns (with in-situ cloud physics). Navy = UW *FIREACE*, Red = NRC *FIREACE*, Green = *VERDI*, Light blue = *ISDAC*, Orange = *MPACE* (And similar for *RACEPAC*), Purple = *SORPIC*, Yellow = *ARCTAS*, Teal = *ACCACIA*, Pink = *ARCPAC*. Grey = *ASTAR*. See Table 1 for project details.



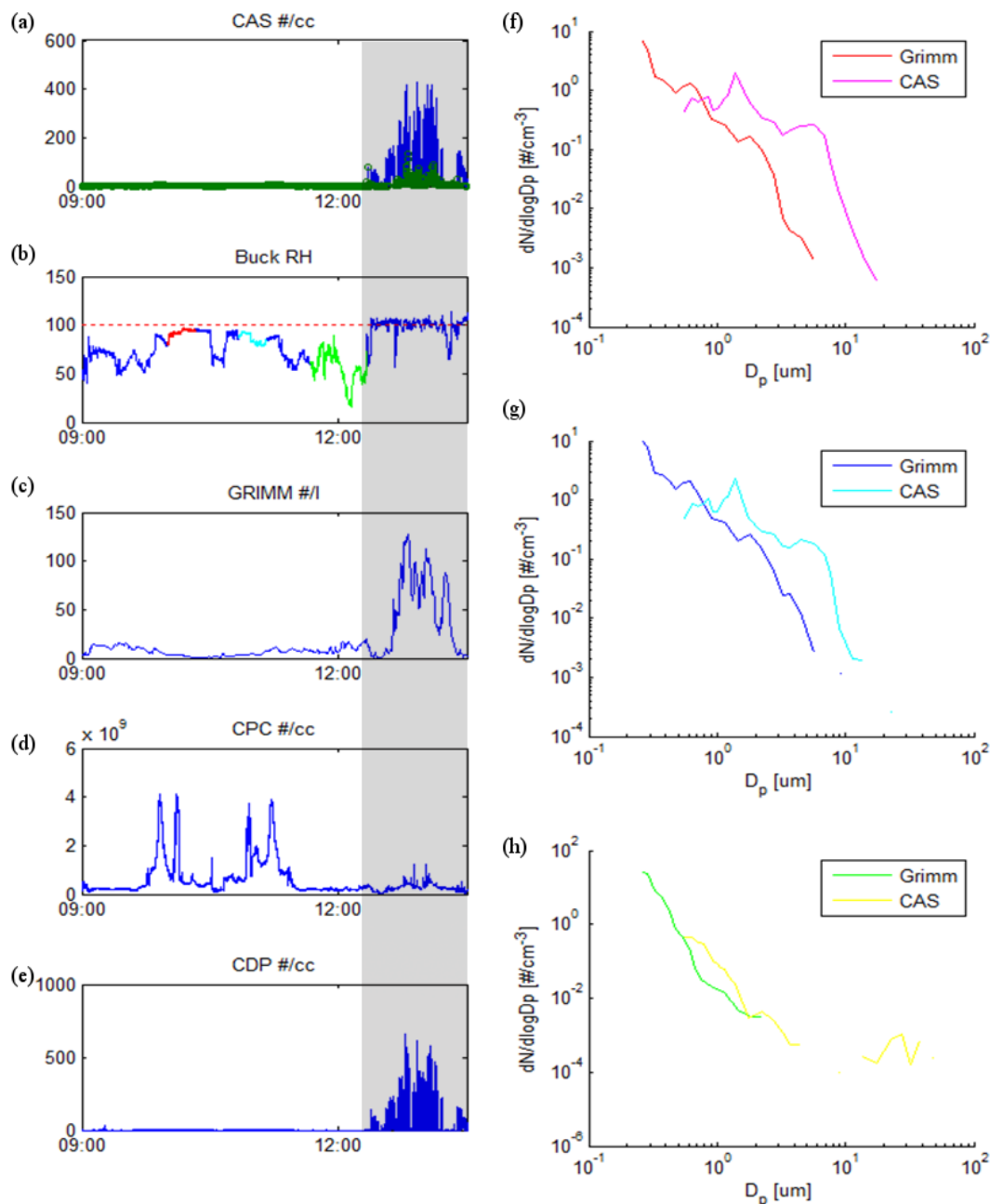
5

Figure 2: Flight tracks for summer ACCACIA flights. Note that M191, the start of M192, M194 and M196 are co-located. Sea ice cover corresponding to flight M195 is shown as a percentage. Separate plots for each flight are included in Fig. S3.



5

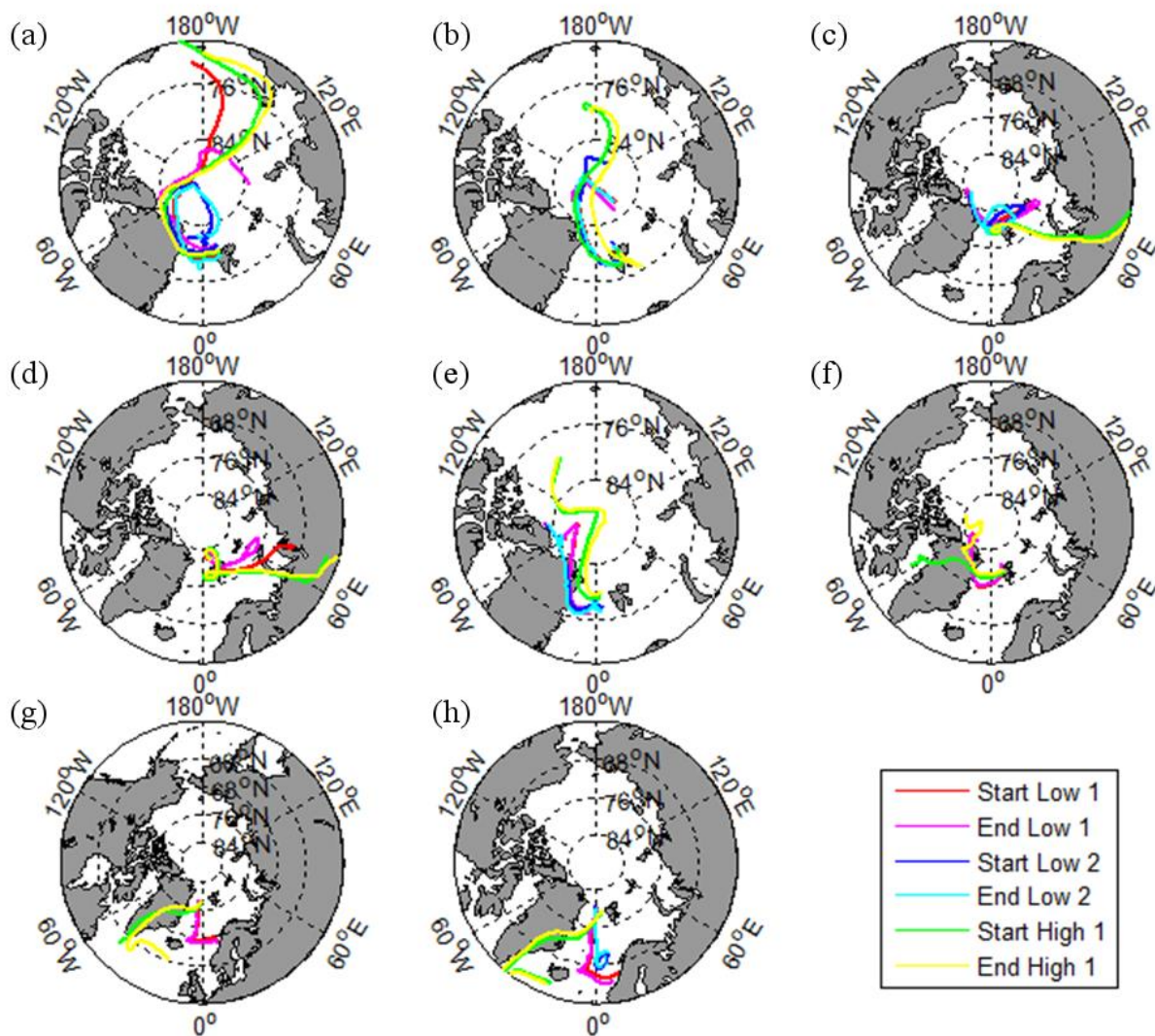
Figure 3: Mean Sea Level Pressure (MSLP) charts (from European Centre for Medium-Range Weather Forecasts (ECMWF) Reanalysis (ERA)-Interim data) showing the synoptic conditions for flight days given in Table 2. White arrows indicate the direction of movement of low pressure centres. Concentric latitude lines are shown at 80 and 70 °N.



5

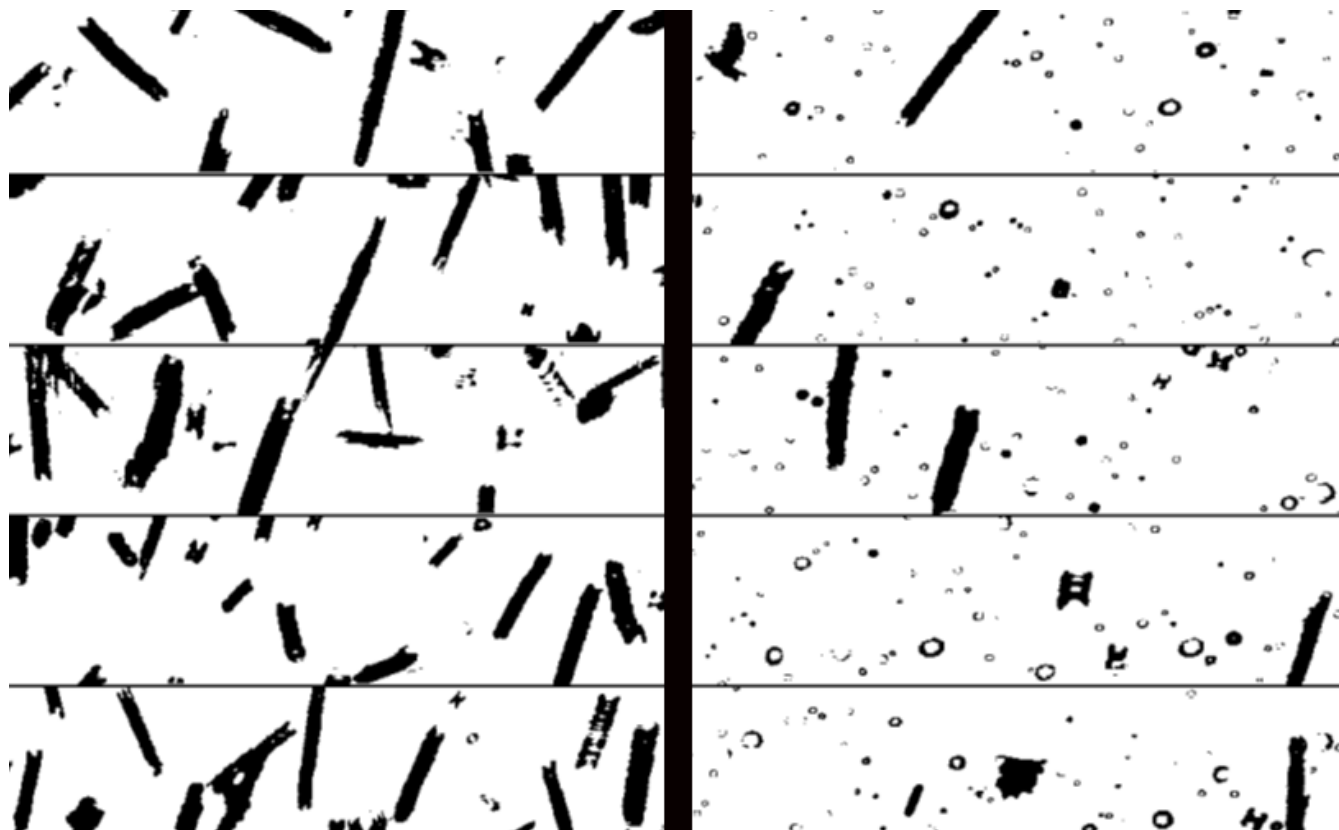
Figure 4: Aerosol data from flight M192. Time series data of a) CAS total concentration (blue) and CAS concentration when CDP concentration was $<1 \text{ cm}^{-3}$ (green), b) RH measured by the Buck instrument, c) GRIMM total concentration, d) CPC concentration, e) CDP total concentration. Shaded area indicates when sampling in cloud (CDP LWC $> 0.01 \text{ gm}^{-3}$). On b) two time periods are highlighted in red and cyan showing low altitude SLRs, and in green showing a high altitude SLR. Mean size distribution data from the CAS and GRIMM during these times are shown in f) and g) for the lower altitude, high RH SLRs and h) for the higher altitude, low RH case.

10



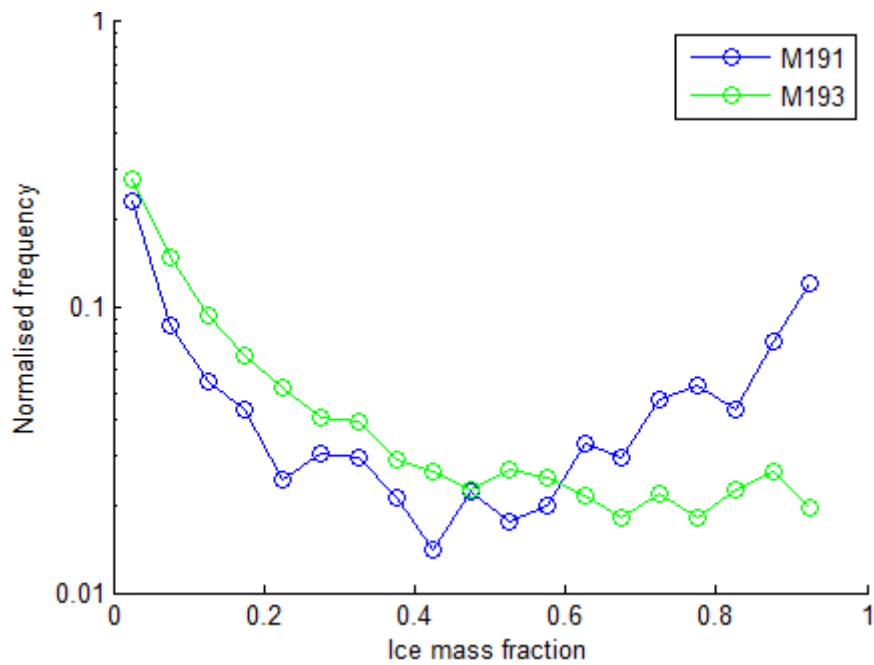
5

Figure 5: HYSPLIT back trajectories from the start and end of the aerosol straight and level runs listed in Table 3. Plots a) – h) represent flights M191 – M198 respectively. Note that not all flights have more than one low altitude run. Also note that short back trajectories do not necessarily mean a low dwell time, as low altitude trajectories are only plotted until intersection with the ground.



5

Figure 6: Images from the 2D-S showing columns from a) M191 at 09:15:06 when the temperature was $-3\text{ }^{\circ}\text{C}$, and from b) M193 at 12:51:05 when the temperature was $-3.8\text{ }^{\circ}\text{C}$.



5

Figure 7: The frequency distribution of the cloud ice mass fraction as measured by the 2D-S for M191 and M193 (in science area only).

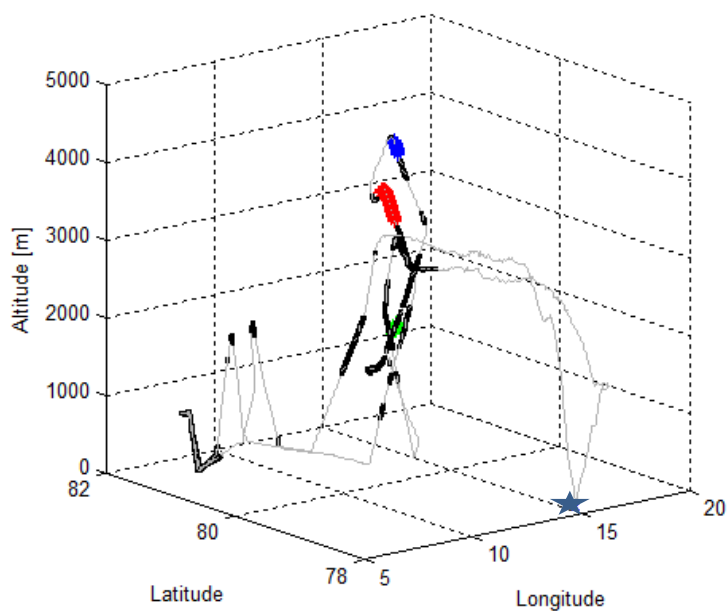
10



5

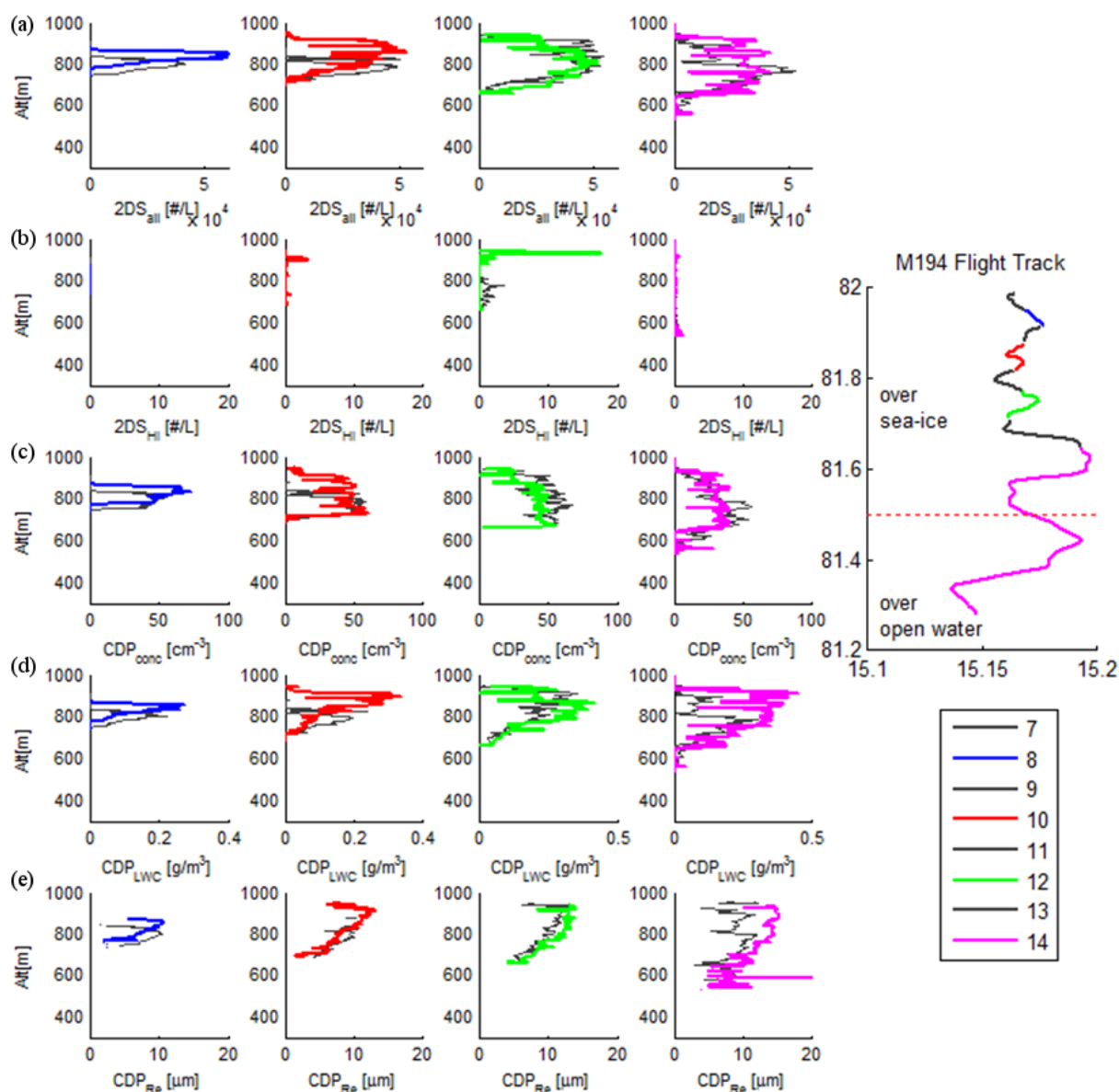
Figure 8: 2D-S images from three occasions when stellar crystals were detected during M193 at a) 12:32:37 – 12:33:26, b) 12:22:07 – 12:25:25 and c) 12:45:01 – 12:46:01 (in order of decreasing altitude, where the most riming is noted for c). See Fig. 9 for location within cloud.

10



5

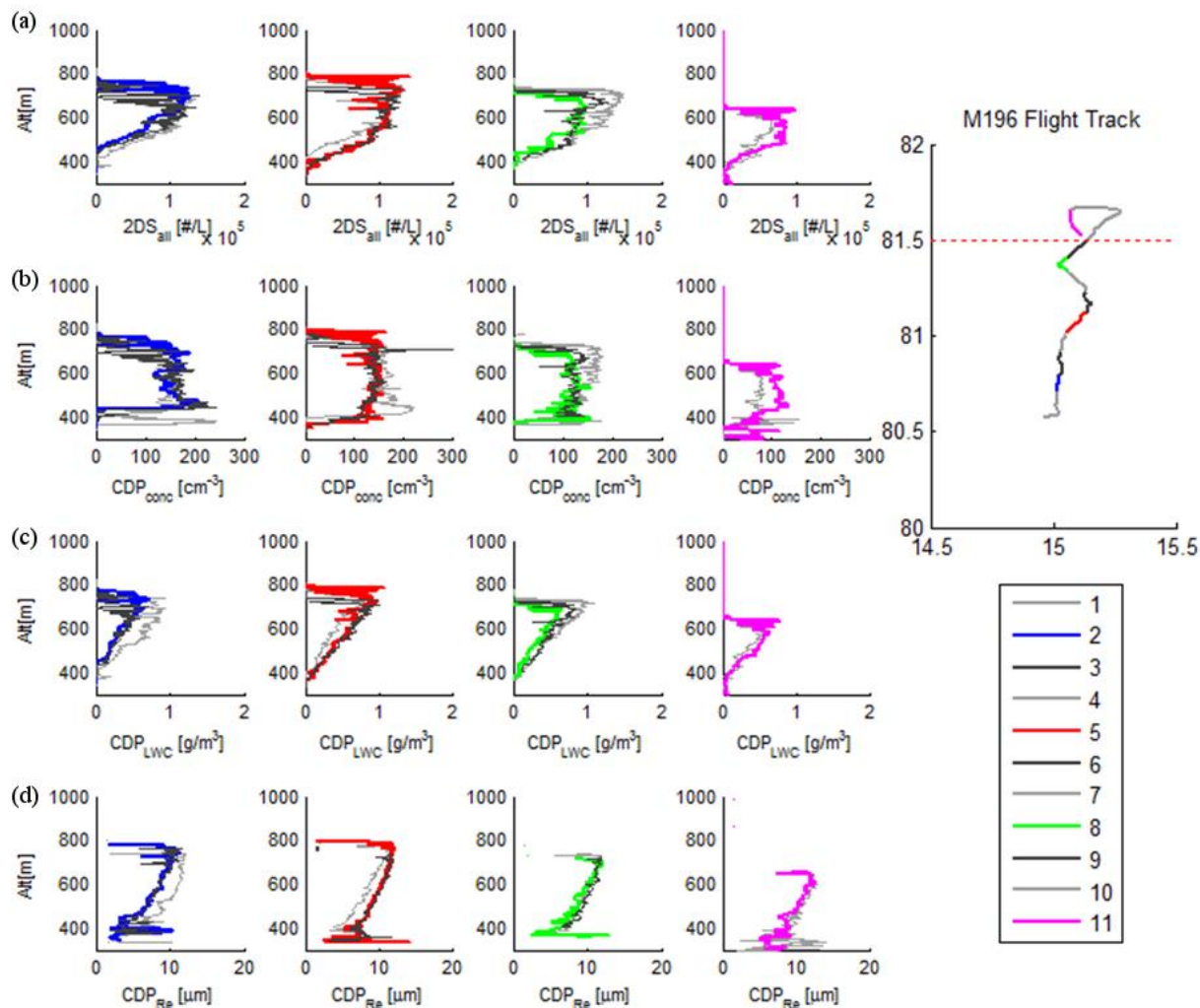
Figure 9: Flight track for M193. Full flight track shown in grey. Cloud presence (determined by CDP LWC > 0.01 gm⁻³) shown in black. Times when stellar crystals were observed shown in blue (12:22:07 – 12:25:25, red (12:32:37 – 12:33:26) and green (12:45:01 – 12:46:01). The blue star indicates the location of Longyearbyen Airport.



5

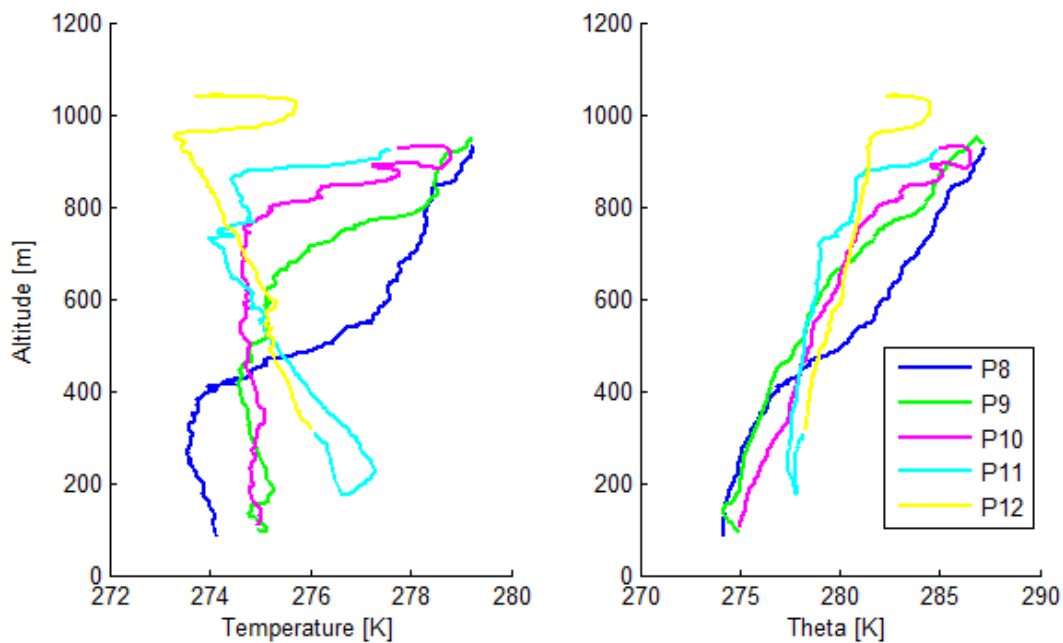
Figure 10: Data from successive profiles through cloud during flight M194. Row a) 2D-S total number concentration, row b) 2D-S HI category only (ice), row c) CDP concentration, row d) CDP LWC, row e) CDP R_e . Flight track on the right indicates where along the flight track the profile data were taken, colours correspond to those shown in the graphs and legend. Additional profiles are shown in black to show the full data available. Aircraft was moving from north to south. Red dashed line on the map indicates the approximate location of 50% ice coverage based on NSIDC data.

10



5

Figure 11: Data from flight M196. Row a) 2D-S total number concentration, row b) CDP concentration, row c) CDP LWC, row d) CDP R_e . The flight track is shown on the right to indicate where along the flight track the profile data were taken. Aircraft was moving from south to north. The red dashed line indicates the approximate location of 50% ice coverage based on NSIDC data.



5

Figure 12: Air temperature (a) and potential temperature (b) profiles for several profiles during M197. The legend details the profile numbers where the latitude and longitude locations of these profiles were: P8 – 77.4° N, 4° W to 3° W, P9 – 77.4° N, 3° W to 2° W, P10 – 77.4° N, 2° W to 1° W, P11 – 77.4° N to 77.6° N, 1° W to 0.5° W, P12 – 77.6° N – 77.1° N, 0.5° W to 0.5° E.

10